International Journal of Biological Macromolecules 340 (2026) 150233

Contents lists available at ScienceDirect

International Journal of Biological Macromolecules

journal homepage: www.elsevier.com/locate/ijbiomac

Effect of anions, concentration and mechanical stimulation on the gelation of agarose

Lorenzo Mio [a], Francesco Piazza [b], Michela Abrami [c], Martina Conti [d], Francesco Lopez [e], Emiliano Fratini [f], Mario Grassi [c], Francesco Brun [c], Ivan Donati [b], Pasquale Sacco [b,*]

[a] Department of Medicine, Surgery and Health Sciences, University of Trieste, I-34129, Trieste, Italy
[b] Department of Life Sciences, University of Trieste, Via Licio Giorgieri 5, I-34127, Trieste, Italy
[c] Department of Engineering and Architecture, University of Trieste, Via A. Valerio 6/1, I-34127, Trieste, Italy
[d] CNR-Istituto Officina dei Materiali (IOM), SS 14 km 163.5, Area Science Park Basovizza, Trieste, I-34149, Italy
[e] Department of Agricultural, Environmental and Food Sciences (DiAAA) & CSGI, Università degli Studi del Molise, Via De Sanctis, I-86100, Campobasso, Italy
[f] Department of Chemistry "Ugo Schiff" & CSGI, University of Florence, Via della Lastruccia 3, I-50019, Sesto Fiorentino (FI), Florence, Italy

ARTICLE INFO

Keywords:
Agarose
Hofmeister effect
Gelation process

ABSTRACT

In this contribution, we report the effect of two anions with different degrees of hydration, namely sulphate (SO_4^{2-}) and chloride (Cl^-), on the gelation of a low hydrophobic agarose (residual methylation = 7.4%). Using a combined approach of oscillatory rheology, low-field NMR, small-angle X-ray scattering (SAXS) and cryo-SEM, we propose that the addition of anions affects water molecules around agarose, causing general dehydration of the biopolymer. This results in earlier temperature of gelation, T_{gel}, less water-biopolymer interactions and greater elasticity of the network at the end of the gelation stage. Mechanical differences level off at the end of the pseudo-equilibrium stage, that is, after 24 h of incubation of the hydrogels at $T = 37$ °C. This causes also low sensitivity of the hydrogels to high ionic strength, which can be explained mainly by the residual amounts of hydrophobic domains of the agarose used in this study. In addition, this contribution provides insights into the role of the agarose concentration, C_p, during the gelation stage. We demonstrate that the established correlation between C_p, network elasticity, and T_{gel} can be related to the extent of interactions between water and agarose. Finally, we discuss the mechanical stimulation of agarose during the gelation stage in the presence of the highly hydrated SO_4^{2-} anion. We report that increasing the oscillatory strain during temperature sweep experiments has negligible effects on T_{gel}, but alters the evolution of the storage modulus on cooling.

1. Introduction

Agarose is the main polysaccharide component of commercial agar-agar, which is obtained from marine red algae, particularly those belonging to the *Gracilariaceae* or *Gelidiaceae* family. Chemically, it consists of repeating units of 3-linked β-D-galactopyranose and 4-linked 3,6-anhydro-α-L-galactopyranose [1], although some substitutions, such as sulphated or methylated sugar dimers, may occur naturally [2,3]. Such substitutions modify the original sequence of the native agarose, although the alternation of 3-linked β-D residues and 4-linked α-L residues is maintained, impacting on the physical properties of the final hydrogels [4]. In addition, chemical modifications such as the introduction of carboxylic acid groups along the agarose backbone have also been proposed in recent years [5].

Agarose undergoes thermally reversible gelation when hydrogen bond-controlled junctions are formed between the biopolymer chains leading to their aggregation, sustained by the entropy gain associated to the release of water molecules from the biopolymer [3,6]. Spinodal decomposition [7–9] or nucleation and growth [10] have been discussed as mechanisms to trigger the gelation of agarose. There is a consensus that agarose gels during cooling in a three-step process: induction, gelation and pseudo-equilibrium stage [10]. After an initial nucleation step, a biphasic transition occurs in the gelation phase: agarose chains initially link to form double-stranded helices to form a weak network. This network then gradually strengthens as the double helices aggregate into bundles, a process that is driven by the cooling - and therefore hydrogen bonds formation - of the original network [11–14]. This biphasic transition is difficult to observe experimentally during the

* Corresponding author.
E-mail address: psacco@units.it (P. Sacco).

https://doi.org/10.1016/j.ijbiomac.2026.150233
Received 17 September 2025; Received in revised form 9 January 2026; Accepted 11 January 2026
Available online 12 January 2026

gelling stage. Final agarose hydrogels appear as slightly turbid, rigid and viscoelastic networks whose mechanics can be well tailored depending on the molecular weight and chemical composition of the agarose, its concentration, the temperature quenching of the solutions and the thermal history of the final hydrogels [4,10,15–19]. Tailored-made agarose hydrogels can be used for the development of cell spheroids [20–22] or in the context of tissue engineering or mechanobiology [17,23–30].

The development of the double helix model has been proposed following X-ray diffraction measurements, optical rotation calculations and sol-gel transition results, which have collectively indicated that each agarose chain forms a left-handed 3-fold helix of pitch 1.90 nm and is translated axially relative to its partner by exactly half this distance [3]. Importantly, the double helix exhibits an interior cavity with a diameter of about 0.45 nm which is expected to be occupied by water molecules, participating in a hydrogen bonding system that contributes to the stability of the double helix. However, the arrangement of double helices does not represent, alone, the stable configuration of the network at low temperatures, where bundles are present. Here, a lateral assembly of helices is required, with at least six double helices forming a cooperative basic unit that can eventually aggregate much more [31]. Nevertheless, it appears that agarose hydrogels are composed of bundles of different thicknesses, and the structure of such bundles may in principle depend on experimental variables such as the concentration of the biopolymer or the quenching rate used in the cooling process. More recent studies using sophisticated spectroscopic techniques such as Raman Optical Activity (ROA) have contributed to elucidate that native agarose hydrogels exhibit, beside double-stranded helix structure, single stranded domains in 60:40 ratio [5]. Considering all these aspects together, there is a crucial contribution of water competing for the formation of hydrogen bonds to chain-chain or helix-helix association, which in principle is expected to modify the gelling process, despite the fact that in a typical hydrogel system there is an overwhelming imbalance of water over biopolymer content, typically of the order of 99:1% w/w.

In this work, we primarily examine the ability of hydrated, *i.e.* kosmotropic, anions to challenge the interplay between the biopolymer and water, providing insights into the gelling mechanism of agarose. We present a combined approach using spectroscopic, scattering, mechanical, and microscopy techniques to investigate both the gelation and pseudo-equilibrium stages. Additionally, we examine the effect of biopolymer concentration and mechanical stimulation on modulating the gelation of agarose.

2. Materials and methods

2.1. Materials

Agarose was purchased from Euroclone (Italy) (code EMR920500). The physical/chemical characteristics of the agarose are the following: total content of agaropectins (in terms of ashes) = 0.6% w/w; gelling temperature = 34 °C; rotational viscosity at 60 °C = 14 mPa s; total methylation = 7.4% determined by ^{1}H- and ^{13}C-HSQC [4]. Another agarose sample from *Gelidium*, with a total agaropectin content (in terms of ashes) of 3.9% w/w, gelling temperature of 33 °C, rotational viscosity at 60 °C of 15 mPa s, and total methylation of 15.5%, was used for comparison in a control experiment (see Fig. S5 in the Supplementary Materials). Sodium chloride (NaCl), sodium sulphate (Na_2SO_4), ammonium sulphate ($(NH_4)_2SO_4$) and ammonium chloride (NH_4Cl) were purchased from Sigma (St. Louis, MO, USA) and from VWR (Italy).

2.2. Preparation of agarose and anions solutions

Agarose powder was dissolved in deionized water to twice the desired final concentration. The mixtures were sealed in a glass vial and autoclaved at T = 121 °C for 15 min. This step is necessary to molecularly disperse the agarose so that it becomes single-stranded coils [31]. Two different anion solutions containing chloride, Cl^-, or sulphate, SO_4^{2-}, were prepared in deionized water at twice the desired concentration. 5 mL of each anion solution was transferred to separate 15 mL Falcon tubes and incubated at T = 60 °C for 15 min, that is "incubation step". Similarly, the autoclaved agarose solution is incubated in same experimental conditions, *i.e.* T = 60 °C for 15 min. After incubation, 5 mL of the agarose solution was added to each anion solution or deionized water used as control ensuring thorough mixing. The final concentration of agarose was in the range 0.5% w/V to 2% w/V, while the concentration of salts containing the anions was 1 M for NaCl or NH_4Cl, and 0.33 M for $(NH_4)_2SO_4$ or Na_2SO_4.

2.3. Oscillation temperature sweep experiments

Oscillation temperature sweep experiments were performed by means of a controlled stress rheometer HAAKE MARS III. A titanium plate with 2° cone/plate geometry (Ø = 35 mm) and a gap of 0.105 mm were used for the setting of experiments. A solvent trap was used to prevent evaporation. After the incubation step at T = 60 °C for 15 min, 500 μL of agarose solutions containing anions or not were poured atop the lower plate (pre-warmed at T = 60 °C). Next, the experiments were carried out under strain-controlled conditions and at a fixed frequency, ν, of 1 Hz, kept constant throughout the measurement. The experiment started at T = 60 °C, with a decrease of temperature of 1 °C/min as previously described [13]. T_{gel} is determined experimentally and corresponds to the onset of the increase in the storage modulus with temperature relative to the baseline [32]. In our set of experiments, the baseline is set to G' = 1 Pa.

2.4. Preparation of cylindrical hydrogels

Agarose hydrogels were formed through an in-well gelation method. After the incubation step at T = 60 °C for 15 min, agarose solutions containing anions or not were poured into a 6-well plate (3 mL/well) and quenched at room temperature (RT) for 30 min. The hydrogels were then incubated at T = 37 °C for 24 h under water-saturated conditions to prevent solvent evaporation [17]. Before rheological analysis, gel disks (20 mm in diameter) were punched out. Additionally, a set of experiments was designed to investigate the effect of soaking of the hydrogels in the anions solution. Here, a 1% w/V agarose solution (deionized water as solvent) was poured into a 6-well plate and allowed to gel at RT for 30 min, as described above. The hydrogels were then transferred to a 45 mm petri dish and soaked in 12 mL of solutions containing SO_4^{2-} or deionized water, used as control. The hydrogels were left soaking at RT for 24 h. Before rheological analysis, 20 mm disks were prepared by punching the hydrogels.

2.5. Rheological characterization of cylindrical hydrogels

A cross-hatched parallel plate-plate apparatus "HPP20 profiliert" with a 20 mm diameter and an operating T = 25 °C were used throughout the conditions tested. To avoid water evaporation from hydrogels, measurements were performed in a water-saturated environment formed by using a glass bell (solvent trap) containing a wet cloth. In addition, to prevent both wall-slippage and excessive hydrogel squeezing, the gap between plates was adjusted by executing a series of short stress sweep tests (τ = 1–5 Pa; ν = 1 Hz) until a constant G' was reached. Then, long stress sweep experiments (τ = 1–1000 Pa; ν = 1 Hz) were conducted.

2.6. Low-field nuclear magnetic resonance (LF-NMR) relaxometry

LF-NMR characterization was performed at T = 25 °C by means of a Bruker Minispec mq20 (0.47 T, Germany). The determination of the average water protons transverse (spin-spin) relaxation time (T_{2m}) was

performed according to the CPMG sequence (Carr–Purcell–Meiboom–Gill) [33] {90°[− τ-180°- τ (echo)]n-T_R} with a 8.36 μs wide 90° pulse, $\tau = 250$ μs, and T_R (sequences repetition rate) equal to 15 s. The criterion adopted to choose n consisted in ensuring that the final FID intensity was about 2% of the initial FID intensity (in the light of this acquisition strategy, we verified that it was un-necessary adopting $T_R > 15$ s). Each measurement was the average of four repetitions. Finally, each FID decay, composed by n points, was saved and analyzed. The relaxation times distribution (A_i, T_{2i}) was determined by fitting the FID time decay (I_s), related to the extinction of the x–y component of the magnetization vector (M_{xy}), according to its theoretical estimation $I(t)$ [34]:

$$I(t) = \sum_{i=1}^{m} A_i \exp(-t/T_{2i});\ T_{2m} = \sum_{i=1}^{m} A_i T_{2i} \Big/ \sum_{i=1}^{m} A_i \quad (1)$$

where t is time, A_i are the pre-exponential factors (dimensionless) proportional to the number of protons relaxing with the relaxation time T_{2i} and T_{2m} is the average relaxation time of protons. For its more immediate meaning, the % value of A_i was reported ($A_{i\%}$) in place of A_i value:

$$A_{i\%} = 100 * A_i \Big/ \sum_{i=1}^{m} A_i \quad (2)$$

The number, m, of the relaxation times (T_{2i}) constituting the relaxation time distribution (A_i, T_{2i}) was determined by minimizing the product $\chi^2 * (2\ m)$, where χ^2 is the sum of the squared errors and 2 m represents the number of fitting parameters of Eq.(1) [35]. Samples were left in a warm bath at $T = 60$ °C. Then, one at a time, they were transferred to the LF-NMR, where the temperature was set to 25 °C, to measure the T_{2m} variations induced by cooling and gelation process for 1 h. T_{2m} was measured, for each sample, also after 24 h. As the average magnetic relaxation time, T_{2m}, is highly influenced by both temperature variation and gelation process, a polymeric solution of PEG of the same agarose concentration, not undergoing gelation upon cooling, was also studied as reference (Supplementary Materials, Fig. S1). The comparison of T_{2m} variation between the agarose and PEG solutions allowed enucleating the effect of the gelation process on T_{2m} variations.

2.7. Cryo-scanning electron microscopy (Cryo-SEM) analyses

The analyses were performed at the Facility of Nano Fabrication (FNF) of the CNR-IOM in Basovizza (Trieste, Italy), using a Leo Crossbeam 1540XB FIB/SEM (ZEISS Microscopy, Oberkochen, Germany) equipped with a QUORUM PP3010Z cryo stage. Briefly, 100 μL of agarose-salt solution was poured onto the holes of the "universal cryo stub" (supplied by Quorum Technologies), forming a hemispherical cap-like drop, at the top of the stub, which gelled at RT within 30 min. The stub with the poured hydrogel was then placed in a deionized water bath for 24 h at RT to remove the salts. The next day, the stubs with the hydrogel were transferred to a "standard holder", then inserted into a custom-made ZEISS shuttle and rapidly frozen by immersion in liquid nitrogen. The frozen shuttle was then transferred to the preparation chamber of the cryo stage and held at −140 °C, where a pre-cooled scalpel was used to slice off the hemispherical cap at the top of the hydrogel drop. This exposed the internal portion of the hydrogel in order to analyze its internal microstructure. The sample was then sublimated at $T = -90$ °C for 20 min, followed by 30 s of platinum sputtering at 10 mA before imaging in the SEM chamber. Cryo-SEM micrographs were analyzed using a custom MATLAB-based workflow. Only images at either 5 k× or 10 k× magnification were used, as they provided the best trade-off between field-of-view and structural detail. A first intensity threshold was applied to separate voids from fibres and to compute the global porosity as the fraction of void pixels relative to the total number of pixels in the image. A second fixed global intensity threshold determined empirically was used to isolate only the relevant imaging plane; this enabled the analysis of both the nearest and the lower planes. From both these thresholded images, individual domains were separated using a marker-controlled watershed procedure: the distance transform of the binary mask was inverted, shallow minima were suppressed, and the watershed transform was applied to delineate subregions. For each resulting region, the area (converted to μm^2 using the calibrated pixel size) was extracted. Pores below an unrealistic size threshold were considered artifacts, as many of these occur within the pore walls. All measurements were exported for further statistical analysis.

2.8. Small angle X-ray scattering (SAXS) analyses

SAXS measurements were conducted using the XEUSS 3.0 HR system (Xenocs SA, Sassenage, France) with Cu Kα radiation (λ) as X-ray source. Calibration of the sample to detector distance was performed using silver behenate (d = 58.376 Å) [36]. The scattering intensity, $I(q)$, was recorded using an EIGER2R (1 M model) hybrid pixel photon counting detector (Dectris Ltd., Baden, Switzerland) consisting of 1028 × 1062 pixels with a size of 75 × 75 μm^2 positioned 400 and 1800 mm far from the sample with collimation in high flux mode. This set-up results in a scattering vector (q) range of 0.006 $Å^{-1} < q < 0.8\ Å^{-1}$ (*i.e.* $q = 4p/l$ sinq where = 1.542 Å and 2q is the scattering angle). The exposure time was in the range 300–1200 s depending on the sample-to-detector distances. In the case of this set of measurements, agarose was dissolved using a dry bath incubator operating at $T \sim 95$ °C for 30 min. Then, the agarose was treated as discussed above for the preparation of solutions containing anions or not (see paragraph 2.2). The preformed hydrogels were loaded into demountable cell of 1 mm thickness with Kapton foils as windows while high temperature agarose dispersions for the investigation of the gelation kinetics were loaded into disposable 2 mm diameter borosilicate glass capillaries (WJM-Glas/Muller GmbH, Berlin, Germany) sealed with hot glue. A Peltier system was used to control the temperature in the range from 15 to 60 °C. The two-dimensional (2D) scattering patterns were radially averaged to obtain $I(q)$, corrected for the corresponding background scattering (empty capillary/Kapton foil and water/aqueous salt solution) and converted in absolute intensity using Xsact (Xenocs, SA, Sassenage, France).

2.9. Statistical analysis and software

Statistical comparisons and graphical elaborations were carried out using GraphPad Prism and Igor Pro software. The data distributions were tested for normality using the D'Agostino-Pearson or the Shapiro-Wilk normality test. Parametric or non-parametric tests were then selected to perform the statistics between the different groups. The specific statistics are reported as indicated in the figure captions. The cartoon in Fig. 9 was created with BioRender.com. The Graphical Abstract is accompanied by the following citation: "Created in BioRender. Sacco, P. (2026) https://BioRender.com/dzcgyiy.

3. Results

3.1. The effect of hydrated anions on agarose gelation stage

We hypothesized to modulate the gelation stage of agarose upon cooling while challenging the ternary biopolymer-biopolymer, biopolymer-water, water-water hydrogen bonding system. To achieve this, we chose two anions with increasing kosmotropic effect [38], namely chloride Cl^- (low kosmotropic degree, poorly hydrated) and sulphate SO_4^{2-} (high kosmotropic degree, highly hydrated), which are expected to shift hydrogen bond formation towards chain-chain association. First, we performed a low-field NMR analysis to verify the ability of the anions to effectively bind water molecules. Experimentally, we worked with the same ionic strength for comparison. The medium relaxation time, T_{2m}, of the proton of the water molecules lowers while increasing the kosmotropic nature of the anion, switching from around

2750 ms in deionized water to around 1950 ms in the presence of SO_4^{2-} (Supplementary Materials, Fig. S2). These data confirm that the water molecules interact much more strongly with the SO_4^{2-} anion than with Cl^-.

Next, we undertook oscillatory temperature sweep experiments to study the gelation stage of agarose in the presence of anions with different kosmotropic degree. We adopted a protocol in which liquid agarose samples were poured on the rheometer stage at 60 °C and cooled down slowly at 1 °C/min while measuring the storage modulus as a function of temperature [32]. We observed a non-monotonic sol-gel transition when deionized water was used as the solvent, with a discontinuity in the storage modulus, G', around 300 Pa (Fig. 1a). The trend of the curve is consistent with a previous study [14], but differs from the constant increase of G' detected in other studies [10,39]. Since, in the latter, a different strain was applied during the temperature-oscillatory sweep experiments, we verified the effect of deformation on this particular behaviour. However, in our experimental setting, the discontinuity remains evident within a strain range of 0.1–1% (Supplementary Materials, Fig. S3). As agarose is extremely sensitive to temperature changes, the non-monotonic trend of the storage modulus as a function of temperature can potentially be explained by the different quenching rate and experimental protocols used in these studies. It is striking that the addition of kosmotropic anions anticipates the gelling temperature, T_{gel}, at which G' begins to increase significantly with temperature (Fig. 1b), and broadens the interval of discontinuity in the curve. Indeed, while agarose dispersed in deionized water shows a discontinuity of about 1.5 °C, in the presence of SO_4^{2-} this expands up to 7 °C. Notably, the temperature range marking the discontinuity region is characterized by evident spikes in the phase angle recorded by the rheometer, indicating that the networks are heterogeneous in their macromolecular arrangement (Supplementary Materials, Fig. S4). Moreover, the discontinuity is also observed for another agarose with a different chemical composition (Supplementary Materials, Fig. S5). T_{gel} does not vary when changing the counterion for sulphate (Na^+ instead of NH_4^+) or chloride (NH_4^+ instead of Na^+) anion, clearly indicating that T_{gel} is sensitive to the nature of the anion rather than that of the cation (Supplementary Materials, Fig. S6). Finally, while Cl^- increases mildly the plateau elastic modulus calculated at $T = 25$ °C, G'_p, from ~10 kPa to ~12 kPa, SO_4^{2-} significantly increases G'_p up to ~20 kPa.

The gelation stage in the presence of different anions was investigated from a structural point of view by using Small Angle X-ray Scattering (SAXS) applying a slightly different thermal cycle as in the oscillatory sweep experiment. SAXS accesses the nanoscale arrangement in the agarose chains and has been already used in the past to characterize the structure of physical and chemical gels [40,41] and to follow the gelation kinetics in several cases as for example agarose [12,31]. The evolution of the structure while cooling is shown in Fig. 2a-c for the three different media. In all cases, at high temperature the scattering curve reveals an open polymer conformation in agreement with the good solvent conditions. As the agarose solutions are cooled, the relative scattering intensity increases, especially at low q, showing the development of the gel-like structure. The gelation kinetics can be followed by plotting the scattering intensity value at low q (*i.e.* 0.007 $Å^{-1}$). Fig. 2d shows that in all the investigated cases the structural variation follows a simple sigmoid trend from single polymer coils to structured bundles in line with a two-state cooperative process. Remarkably, the SAXS curves confirm that the sol-gel transition of agarose can be well anticipated as a function of the kosmotropic nature of the anion, with calculated inflection point of 41.2 °C for SO_4^{2-}, 38.9 °C for Cl^- and 36.1 °C for deionized water. No sign of the isolated helix could be assessed by SAXS intensity distribution. This is consistent with a previous study stating that the two steps, consisting of the growth followed by the aggregation of helices, cannot be separated experimentally [31]. This could be linked to several concomitant factors as well as the polydispersity of both the starting agarose batch and the helix generating the bundles, the limited q-vector range accessible in a lab-scale SAXS or the experimental protocol used for the preparation of agarose solutions.

To obtain more information on the role of kosmotropic anions on the gelation stage of agarose, low-field NMR analysis was carried out. In this case, agarose solutions in the absence or presence of anions were loaded at 60 °C and immediately quenched at 25 °C in the instrument. At the beginning of the kinetics, when the cooling effect prevails over the gelation process, the medium relaxation time, T_{2m}, of agarose solutions containing SO_4^{2-}, Cl^-, or in deionized water is 2530 ms, 4040 ms, and 4250 ms, respectively. As gelation proceeds, an exponential decay of T_{2m} is observed for all conditions tested (Fig. 3), leading to a well-established plateau. At the end of the kinetics, *i.e.* at 60 min, this plateau is 3.8-fold and 2.3-fold higher for SO_4^{2-} and Cl^-, respectively, than for the deionized water condition. This indicates that a smaller amount of water interacts with agarose chains in hydrogels containing Cl^-, and even less in those containing SO_4^{2-} [42].

Two different transverse relaxation times can be decoupled from T_{2m}, namely a long one (T_{long}) and a short one (T_{short}) (Fig. 4, upper panel). While T_{long} describes the relaxation of the water molecules in the range of 0–15 min, T_{short} only appears around 7 min with partial overlapping with T_{long}. The presence of two relaxation times in the overlapping region indicates that the water molecules experience two

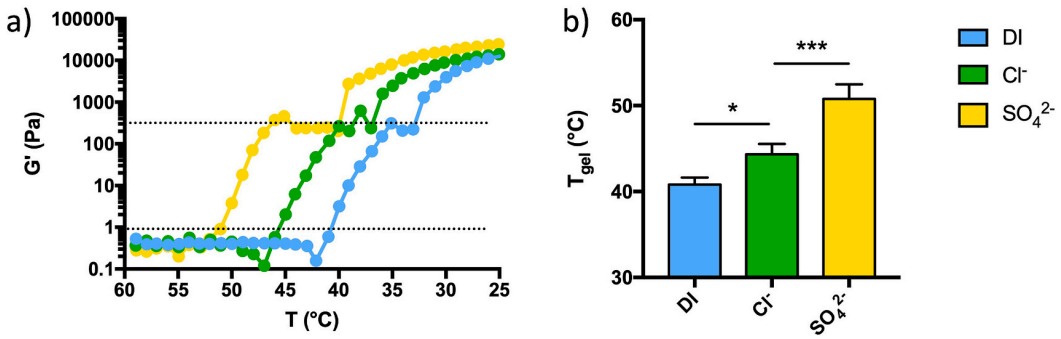

Fig. 1. Effect of anions with different hydration on the elastic response of agarose during the gelation stage. **(a)** Sample-case temperature sweep curves of agarose in the absence or presence of anions Cl^- or SO_4^{2-}. The solid dots and lines represent the experimental values of the storage modulus, G'. The upper dotted line marks the discontinuity in the elastic modulus response around 300 Pa. The lower dotted line is set at 1 Pa and marks the baseline for the calculation of T_{gel}. **(b)** Bar graphs indicating the temperature at which the gelation of agarose starts, T_{gel}, for the three conditions tested; data are given as mean ± SD, $n = 3$–5 samples analyzed for each experimental condition. Statistics: *, $p < 0.05$; ***, $p < 0.001$; One-way ANOVA followed by Tukey's Multiple Comparisons test. The oscillatory temperature sweep experiments were performed with a constant strain of 0.5%, a frequency of 1 Hz and a cooling rate of 1 °C/min. Composition of samples: [agarose] = 1% w/V; deionized water (DI) or anion (Cl^- or SO_4^{2-}) solutions, as dispersing phase. In the case of anion solutions, the ionic strength, I, is kept constant at 1 M, considering also the contribution of the respective counterions (Na^+ for chloride and NH_4^+ for sulphate).

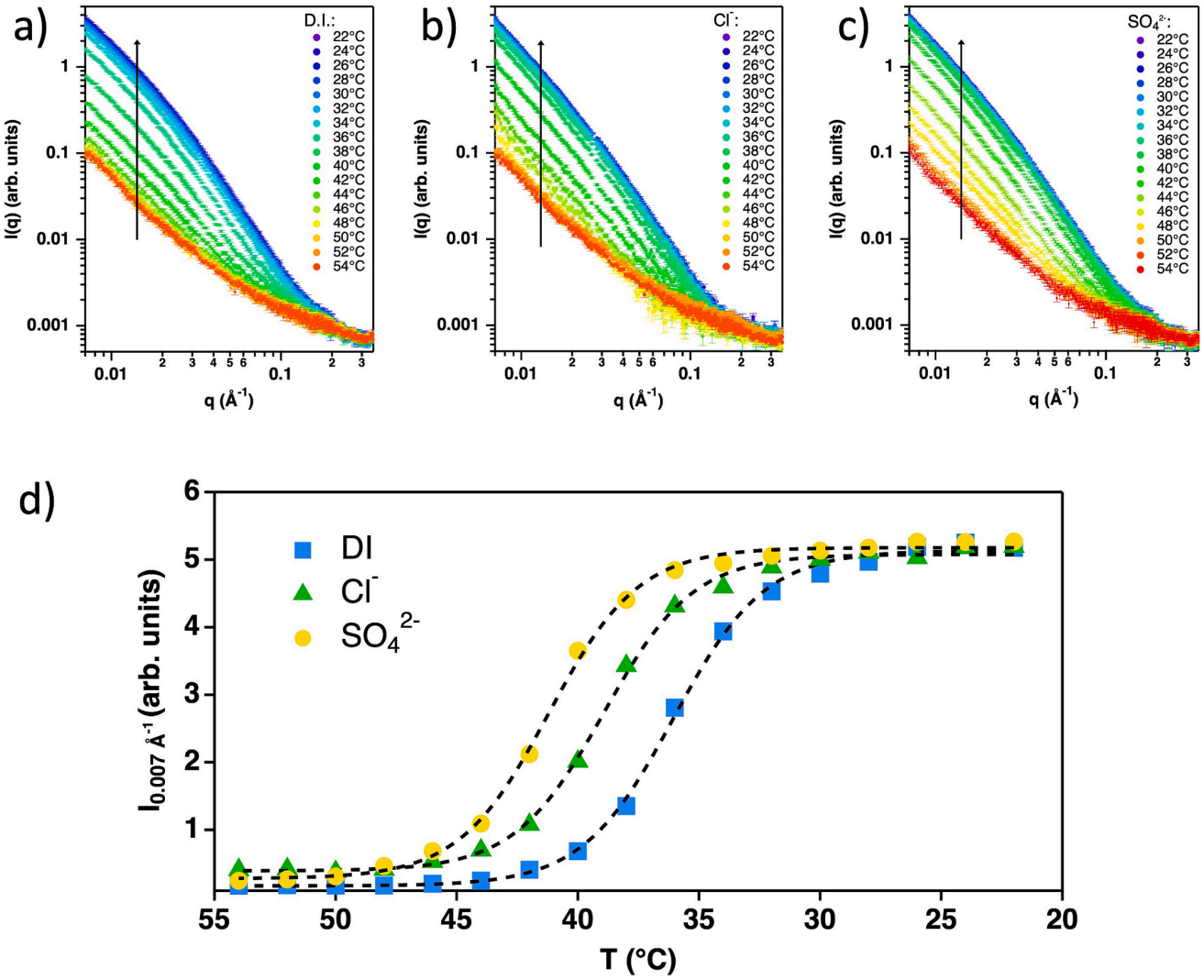

Fig. 2. Nanoscale evolution during the gelation stage of agarose with different anions. Scattering intensity distribution from 54 to 22 °C in the case of agarose solutions: **(a)** DI, **(b)** Cl^- and **(c)** SO_4^{2-}. Black arrows indicate the decrease in temperature. Panel **(d)** shows the evolution of the scattering intensity at low *q* (*i.e.* 0.007 A^{-1}) while cooling the agarose solution in deionized water (DI) or the presence of Cl^- and SO_4^{2-}. Dashed lines correspond to the best fit using a sigmoid function. Composition of samples: [agarose] = 1% w/V; deionized water (DI) or anion (Cl^- or SO_4^{2-}) solutions, as dispersing phase. In the case of anion solutions, the ionic strength, *I*, is kept constant at 1 M, considering also the contribution of the respective counterions (Na^+ for chloride and NH_4^+ for sulphate).

microenvironments characterized by different mobility in the said time frame. Interestingly, the combination of T_{long} with T_{short} follows a well-defined exponential decay for all conditions tested. A more detailed insight into the characteristics of the gelation kinetics of agarose can be obtained by analyzing the spin densities in the critical overlapping time window of 0–20 min, which is associated with the long and short relaxation times, *i.e.* A_{long} and A_{short}, respectively (Fig. 4, lower panel). As for the gelation kinetics, the progressive changing of two microenvironments of water molecules is clearly observed in the case of pure deionized water in the above interval. When the poorly hydrated anion Cl^- is added, the spin densities are more scattered but evolve similarly. In the case of highly hydrated SO_4^{2-} anion the changing of topology's network comes abruptly after an apparent equilibrium phase. Here, only 20% of water molecules with lower relaxation time are observed in the time window of 5–12 min for the short relaxation time, indicating that the majority of water molecules, *i.e.* 80%, which are characterized by higher relaxation time, dominate during the entire investigated time window. However, also in this case, it is important to note that after 12 min, 100% of the water molecules are associated with the short relaxation time, indicating a sole microenvironment. Overall, by combining rheological, SAXS, and LF-NMR data, we conclude that the sol-gel transition of agarose proceeds from individual polymer coils to structured bundles. The addition of anions with varying kosmotropic degree enables dehydration of the biopolymer, advancing the onset of the gelation stage. Notably, the bundles mature into networks characterized by different topology and water-biopolymer interactions depending on the type of anion.

3.2. *The effect of concentration and mechanical stimulation on agarose gelation stage*

Next, we varied the overall concentration of agarose and applied a mechanical stimulation to investigate the gelation stage. Regarding the first approach, we hypothesized that variations in agarose content would promote tuneable entanglement of the biopolymer on cooling modulating the gelation temperature and the plateau elastic modulus. Therefore, we performed oscillatory temperature sweep experiments with constant amplitude and varying amount of agarose, C_p, using

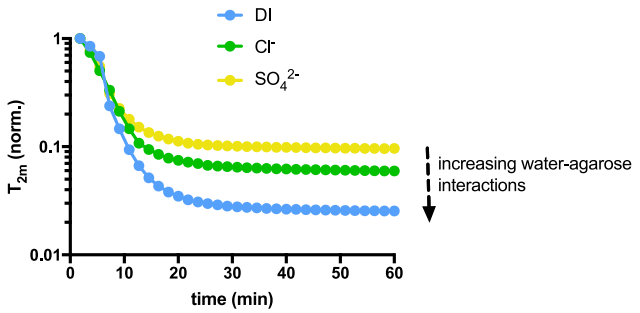

Fig. 3. Anions with different hydration promote the formation of hydrogel networks with different water-biopolymer interactions. Dependence of the normalized medium relaxation time, T_{2m}, of the proton of the water molecules during the gelation stage of agarose. The low-field NMR experiments were performed immediately quenching the samples at $T = 25$ °C. Composition of samples: [agarose] = 1% w/V; deionized water (DI) or anion (Cl^- or SO_4^{2-}) solutions, as solvent. In the case of anion solutions, the ionic strength, I, is kept constant at 1 M, considering also the contribution of the respective counterions (Na^+ for chloride and NH_4^+ for sulphate).

deionized water as solvent. A non-monotonic increase of the storage modulus as a function of temperature is observed for all condition tested, with the presence of a discontinuity range around 300 Pa (Fig. 5a). We found a mild power-law dependence when T_{gel} is correlated with C_p, with $T_{gel} \propto C_p^{0.2}$ indicating that the influence of biopolymer concentration is weak for the onset of gelation (Fig. 5b). Conversely, the dependence of the plateau elastic modulus on the agarose content is noteworthy, with $G'_p \propto C_p^{2.4}$ for $C_p \geq 1\%$ w/V, and a progressive increase of slope for $C_p < 1\%$ w/V (Fig. 5c). The trend of the plateau elastic modulus as a function of C_p is consistent with previous findings by Morris and co-workers, where the calculated exponent was approximately 2 [13].

The correlation between the plateau elastic modulus and agarose content for $C_p \leq 1\%$ w/V was also studied by LF-NMR. An exponential decay of T_{2m} is observed for all conditions tested, although higher variability is detected for $C_p = 0.5\%$ w/V (Fig. 6a). At the end of the kinetics, T_{2m} is 2.5-fold and 1.7-fold higher for $C_p = 0.5\%$ w/V and $C_p = 0.75\%$ w/V, respectively, than for $C_p = 1\%$ w/V, which is used as a reference. This indicates that weaker water-polymer interactions take place in hydrogels with $C_p = 0.75\%$ w/V, and even less in those with $C_p = 0.5\%$ w/V. Indeed, this is coherent with the decreasing polymer-water interface in less concentrated hydrogels. The correlation between T_{2m} and C_p is shown in Fig. 6b, and results $T_{2m} \propto C_p^{-1.3}$. Importantly, the spin densities derived from the two decoupled relaxation times, namely T_{long} and T_{short}, show the presence of a heterogeneous network composed of two microenvironments with different water content for hydrogels with $C_p = 0.5\%$ w/V, and a single network for $C_p = 0.75\%$ w/V at the end of the kinetics (Supplementary Materials, Fig. S7).

Considering the extended discontinuity range of the storage modulus of agarose in the presence of SO_4^{2-} compared to the pure solvent (Fig. 1a), we wondered whether variable mechanical stimulation would modulate the gelation stage of the biopolymer. Therefore, we changed the amplitude imposed on the rheometer during oscillatory temperature sweep experiments. All samples analyzed exhibit a discontinuity region around 300 Pa, the extent of which can potentially be modulated, within the limits of high experimental error, by the magnitude of the oscillatory

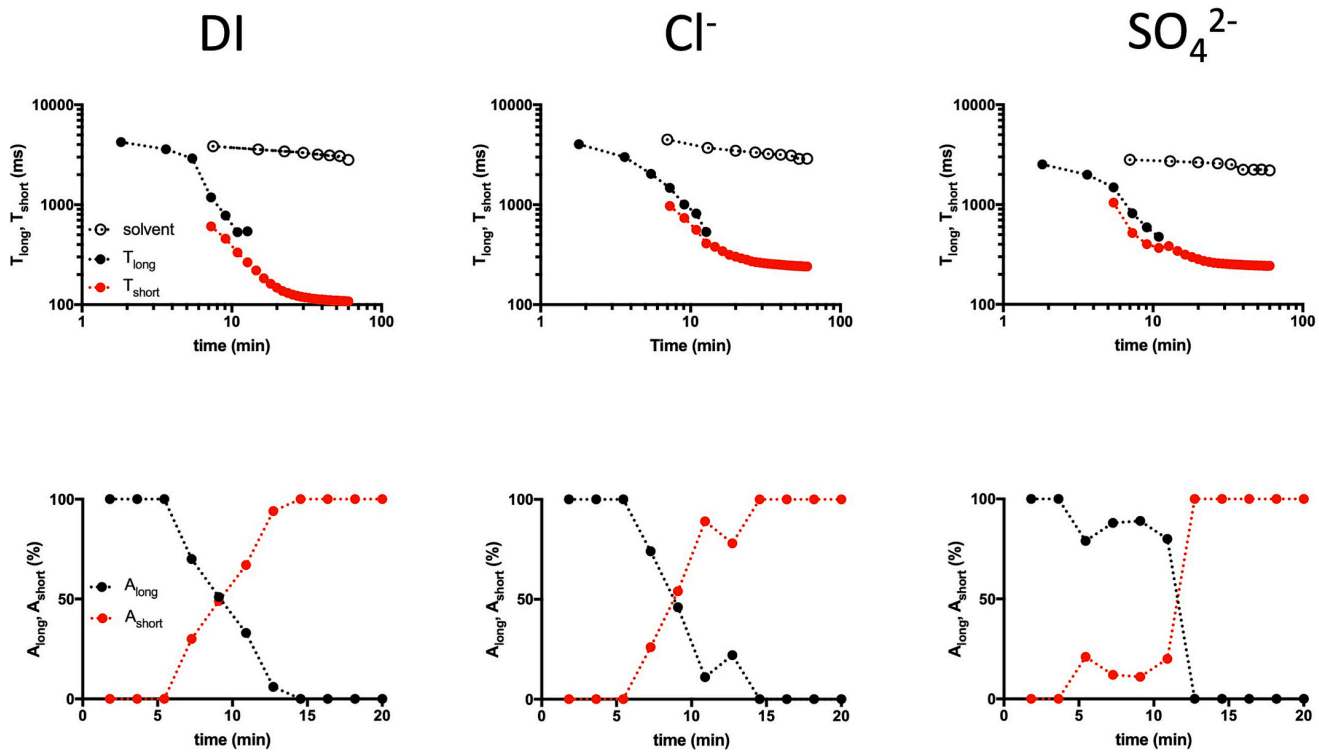

Fig. 4. Effect of anions with different hydration on the evolution of the topology network during the gelation stage of agarose. Upper row: dependence of the long (T_{long}) and short (T_{short}) relaxation time during the hydrogel formation; the empty dots represent the experimental points associated with solvent as reference; the dotted lines are drawn to guide the eye. Lower row: variation of the spin density of the signal in relation to the long (A_{long}) and short (A_{short}) relaxation times; the dotted lines are drawn to guide the eye. The low-field NMR experiments were performed immediately quenching the samples at $T = 25$ °C. Composition of samples: [agarose] = 1% w/V; deionized water (DI) or anion (Cl^- or SO_4^{2-}) solutions, as solvent. In the case of anion solutions, the ionic strength, I, is kept constant at 1 M, considering also the contribution of the respective counterions (Na^+ for chloride and NH_4^+ for sulphate).

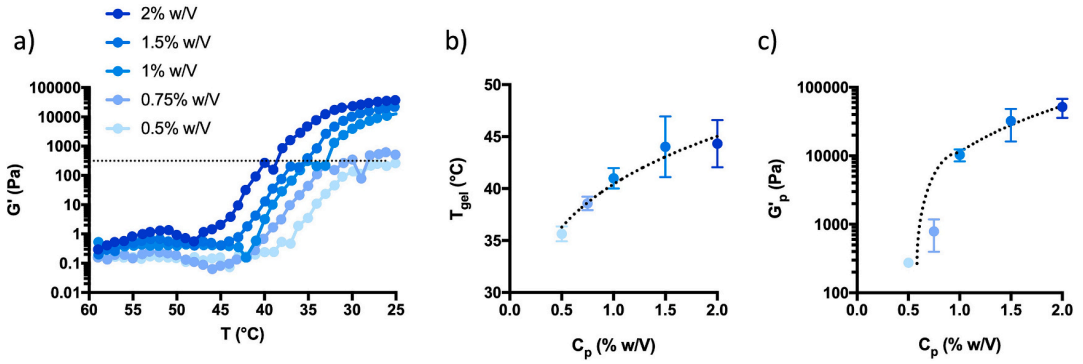

Fig. 5. Effect of agarose concentration on the gelation stage of agarose. **(a)** Sample-case temperature sweep curves of agarose at different concentration. The solid dots and lines represent the experimental values of the storage modulus, G'. The dotted line marks the discontinuity in the elastic modulus response around 300 Pa. **(b,c)** Dependence of T_{gel} and the plateau elastic modulus, G'_p, as a function of agarose concentration (C_p, % w/V); data are given as mean ± SD, n = 2–3 samples analyzed for each experimental condition. The dotted line in plot (b) represent the best fit of the experimental points according to a power-law dependency, *i.e.* $y = ax^b$. The dotted line in (c) is included to guide the eye. The temperature sweep experiments were performed with a constant strain of 0.5%, a frequency of 1 Hz and a cooling rate of 1 °C/min. Composition of samples: [agarose] = 0.5% - 2% w/V; deionized water as solvent.

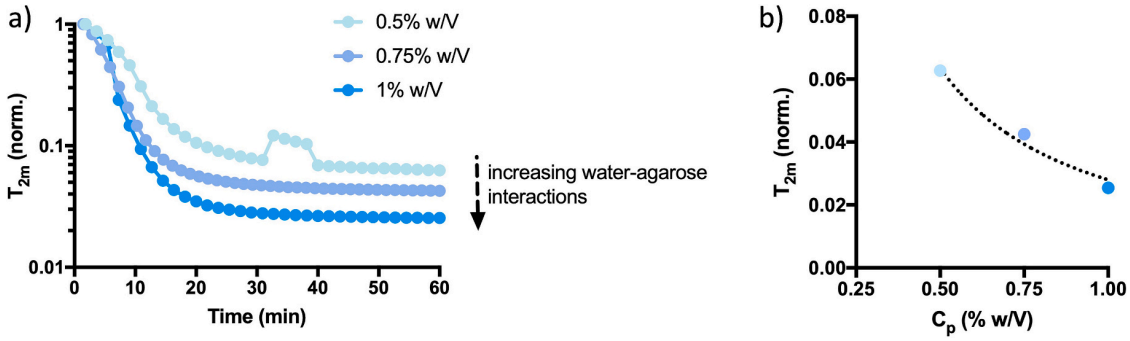

Fig. 6. The concentration of agarose promotes the formation of hydrogel networks with different water-biopolymer interactions. **(a)** Dependence of the normalized medium relaxation time, T_{2m}, during the gelation stage of agarose. **(b)** Dependence of the medium relaxation time, T_{2m}, at the end of gelling kinetics as a function of agarose concentration (C_p, % w/V); the dotted line represents the best fit of the experimental points according to a power-law dependency, *i.e.* $y = ax^b$. The low-field NMR experiments were performed immediately quenching the samples at T = 25 °C. Composition of samples: [agarose] = 0.5–1% w/V; deionized water (DI) as solvent.

shear, showing a negative dependence as a function of imposed strain (Fig. 7a,b). The plateau elastic modulus also scales negatively with the applied strain (Fig. 7c). In contrast, mechanical stimulation has a negligible effect on the gelling temperature, with $T_{gel} = 52 \pm 2$ °C for the different conditions explored. Taken together, these results show that varying the biopolymer concentration as well as mechanical stimulation

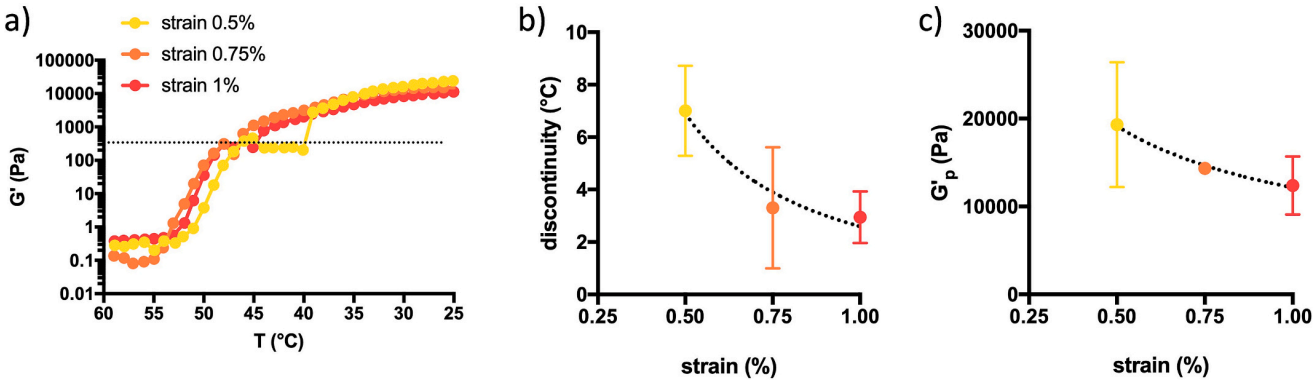

Fig. 7. Effect of mechanical stimulation on the gelation stage of agarose. **(a)** Sample-case temperature sweep curves of agarose performed at different shear strain. The solid dots and lines represent the experimental values of the storage modulus, G'. The dotted line marks the discontinuity in the elastic modulus response around 300 Pa. **(b,c)** Dependence of discontinuity region in the elastic modulus response and T_{gel} as a function of applied strain (%); data are given as mean ± SD, n = 2–3 samples analyzed for each experimental condition. The dotted lines are drawn to guide the eye. The temperature sweep experiments were performed with variable strain as indicated in (a), a frequency of 1 Hz and a cooling rate of 1 °C/min. Composition of samples: [agarose] = 1% w/V; SO_4^{2-} solution as dispersing phase. The ionic strength, I, is 1 M, considering also the contribution of the respective counterion, *i.e.* NH_4^+.

are useful approaches to modulate the gelation stage of agarose.

3.3. The effect of hydrated anions on cylindrical agarose hydrogels at the end of the pseudo-equilibrium stage

Next, we performed a structural characterization at the end of the pseudo-equilibrium stage, *i.e.* after 24 h gelation, on cylindrical agarose hydrogels [10,17]. Rheological strain-sweep experiments were performed to obtain information on the mechanics of cylindrical agarose hydrogels under small and large deformations in the absence or presence of anions with different kosmotropic degree. We found no statistical differences in the shear modulus G - calculated at small deformations - when comparing hydrogels assembled in pure deionized water and in the presence of Cl^- or SO_4^{2-} anions (Fig. 8a). Here G flattens at 9 kPa indicating same stiffness. The determination of T_{2m} by LF-NMR approaches approximately 130 ms for all conditions tested, indicating that the three hydrogels share the same water-biopolymer interactions, that can be intended as similar mesh size. This is consistent with the shear modulus discussed above and with our previous contribution [43]. To provide more information about viscoelastic properties of the hydrogels we calculated the critical strain, γ_c [44], while fitting stress-strain experimental data (Eqs. (3) and (4)) where G corresponds to the shear modulus at $\gamma_{\to 0}$ and b is a fitting parameter:

$$\sigma = \frac{G}{1 + b\gamma}\gamma \tag{3}$$

$$\gamma_c = \frac{0.05}{0.95\, b} \tag{4}$$

This parameter represents the point at which the linear stress-strain regime ends. Although the critical strain is slightly higher in the presence of the anions, no statistical differences were found, suggesting similar viscoelasticity of these hydrogels compared to those formed in deionized water (Fig. 8b). These results reflect the trend for the elastic energy (Fig. 8c), E_e, calculated at γ_c as (Eq. (5)):

$$E_e = \int_{\gamma=0}^{\gamma_c} \left(\frac{d\sigma}{d\gamma}\bigg|_{\gamma=0} \right) \gamma\, d\gamma = \frac{1}{2}\, G\, {\gamma_c}^2 \tag{5}$$

Next, we acquired cryo-SEM images to observe the architecture of the hydrogel networks (Fig. 8d). It is interesting to note that hydrogels prepared in deionized water or in the presence of the poorly hydrated Cl^- exhibit a uniform distribution of the polysaccharide bundles, whereas the presence of the highly hydrated SO_4^{2-} anion slightly alters the architecture of the network and leads to mild packing of the bundles reminiscent of the dehydration process during the gelation stage. The analysis of the pore area and overall porosity in the hydrogel network, however, reveals no statistical difference among the conditions tested (Supplementary Materials, Fig. S8). Details on the architecture of the network in the nanometer-scale can be extracted, also, by the modelling of the SAXS curve of the agarose hydrogels at the end of the cooling process obtained in the presence of the diverse anions as reported in Fig. 8e-g. The scattering pattern can be described by a model consisting of two different contributions: one for the correlation length in the liquid-like region (*i.e.* "blob" or mesh size of the gel, ξ) and the second contribution accounting for the large-scale inhomogeneities or solid-like regions (Guinier radius, R_g). As shown in Table S1 the effect of the different electronic densities on the anions in the aqueous phase results in a mesh size of about 7 nm in the case of DI to about 10 nm in the case of the highly hydrated anion, *i.e.* SO_4^{2-}, with an intermediate value of about 8 nm in the case of Cl^-. The clusters originated from the helix bundles result R_g of about 30–32 nm for DI and Cl^- while slightly larger values are obtained in the case of SO_4^{2-} which induces the formation of cluster with R_g reaching 38 nm. From the rheological, SAXS and cryo-SEM analyses, we conclude that although the highly hydrated SO_4^{2-} anion promotes more densely packed bundles that minimally alter the network architecture, both anions have minimal effect on the mechanical response of agarose hydrogels, especially regarding their elasticity, at the end of pseudo-equilibrium stage.

To investigate the effect of anions towards the sensitivity to mechanical stress of agarose hydrogels, we performed long-stress sweep measurements at increasing ionic strength, I. It is important to recall that in these experimental conditions both the contributions of the cation and the anion are considered in the calculation of ionic strength, giving $I = \frac{1}{2}\sum_i^n C_i Z_i^2$. However, the influence of cations on the overall biopolymer-water interplay is much smaller as demonstrated by us in this study and others [32,38], as they are generally excluded from the interface [45]. Therefore, we discuss the following data in terms of the sole contribution of the anion. First, we verified the effect of low hydrated Cl^- anion (in the form of NaCl salt) on the mechanical properties of agarose hydrogels. Under these experimental conditions, we found an opposite behaviour when comparing G and γ_c as a function of ionic strength. This indicates a mild decrease in the shear modulus and a simultaneous increase in the magnitude of the linear stress-strain response, implying that agarose hydrogels become softer but more stretchy when I is increased (Supplementary Materials, Fig. S9). The parameter E_e also increases, albeit not linearly and with more experimental error, as a function of ionic strength. Secondly, we verified the effect of the highly hydrated SO_4^{2-} anion - in the form $(NH_4)_2SO_4$ salt - on same mechanical features. SO_4^{2-} slightly increases G up to $I = 2$ M, and then dramatically decreases it thereafter. We extrapolated the critical ionic strength at which the elasticity of agarose hydrogels drops, resulting in $I = 2.6$ M. At $I > 2.6$ M, an important salting-out effect begins to predominate, causing a weakening of the network and macroscopically the formation of aggregates that are clearly visible at the naked eye (Supplementary Materials, Fig. S10). Salting-out is further enhanced at $I = 6$ M, an experimental condition that does not favour the formation of a hydrogel network, but only the development of agarose aggregates and massive syneresis. In turn, γ_c increases in the presence of SO_4^{2-} anion up to $I = 3$ M indicating same sensitivity towards applied stress as Cl^-. $I = 4$ M represents the experimental condition where the heterogeneity of the network caused by salting-out permits a more evident extension of the linear stress-strain response. Interestingly, the trend of E_e as a function of ionic strength follows a sigmoidal behaviour, indicating that the elastic energy of agarose hydrogels can be progressively increased while increasing the amount of the highly hydrated anion.

4. Discussion

The gelation of agarose on cooling can be interpreted as a transition from "disorder" to "order", with the disordered state being the solution and the ordered state being the gel. In addition to the formation of hydrogen bonds between the polysaccharide chains with favourable enthalpy change ($\Delta H < 0$), the ordered state is stabilized, in principle, by the very large entropy gain due to the water molecules that are released from the disordered macromolecule during cooling. Overall, we have shown that the gelation stage of agarose can be primarily modulated by using kosmotropic anions, and secondarily by changing the biopolymer entanglement or applying mechanical stimulation. Regarding the use of anions, the modulation of T_{gel} can be explained by different interactions between anions, water and the biopolymer at the molecular level [37]. First, the anions could affect the hydrophobic hydration of the residual hydrophobic domains of the agarose due to changes in the interfacial tension between the biopolymer and the water interface; secondly, the anions could bind directly to the hydrophobic parts of the biopolymer; thirdly, the anions can interact with the biopolymer by changing the entropy of the water molecules around the hydrophilic sites of the agarose. In the latter case, the ability of an anion to polarize the water around the hydrophilic sites of the biopolymer should correlate with the ability of the anion to order the water

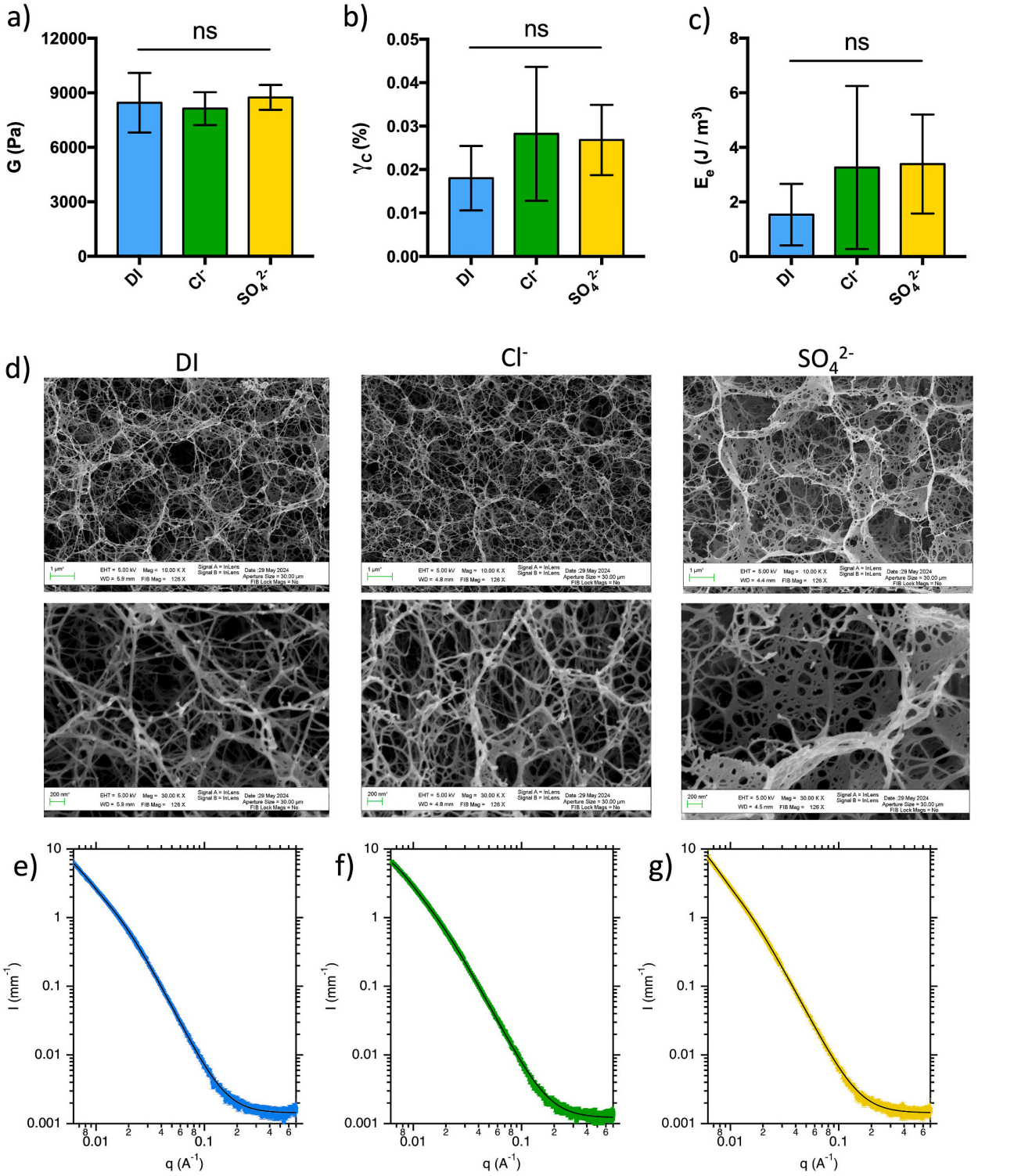

Fig. 8. Effect of anions with different hydration, *i.e.* kosmotropic degree, on the physical properties of agarose hydrogels at the end of pseudo-equilibrium phase. **(a-c)** Bar graphs indicating the shear modulus, G, the critical strain which marks the end of stress-strain linear region, γ_c, and the elastic energy, E_e, calculated at γ_c for the three set of hydrogels investigated; data are given as mean ± SD, $n = 9$–14 hydrogels analyzed for each experimental condition. Statistics: ns, not significant; One-way ANOVA followed by Tukey's Multiple Comparisons test. The long strain sweep experiments were performed at $T = 25$ °C using a frequency of 1 Hz. **(d)** Cryo-SEM images of the internal network for the three set of hydrogels investigated. The scale bar is 1 μm (upper row of images) and 200 nm (lower row of images). **(e-g)** SAXS intensity distribution for the investigated hydrogels. Experimental points are indicated by markers and error bars while the continuous line represents the best fits according to Eq. S1 in the Supplementary Materials file. Composition of hydrogels: [agarose] = 1% w/V; deionized water (DI) or anion (Cl^- or SO_4^{2-}) solutions. In the case of anion solutions, the ionic strength, I, is kept constant at 1 M, considering also the contribution of the respective counterion (Na^+ for chloride and NH_4^+ for sulphate).

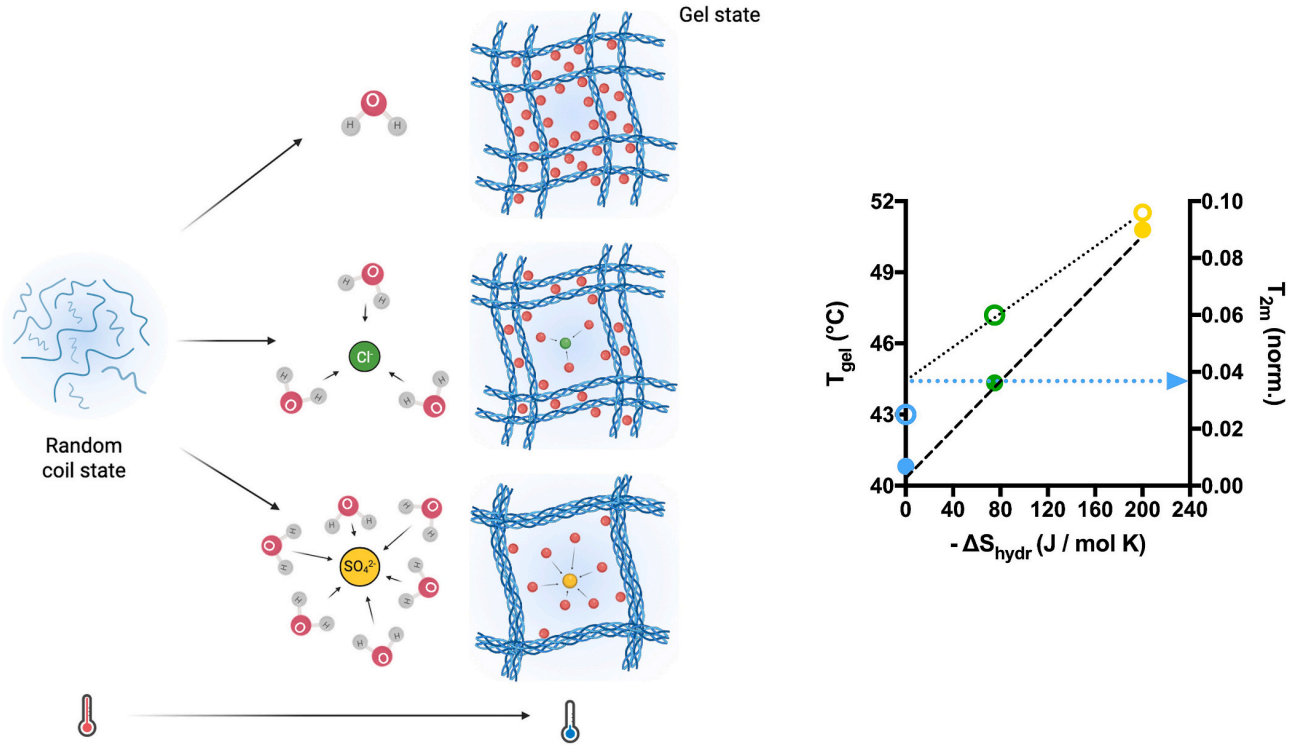

Fig. 9. Tunable sol-gel transition of agarose in the presence of hydrated "kosmotropic" anions. The agarose chains are molecularly dispersed in the hot solution in a random coil, "disordered" state. On cooling, the sol-gel transition occurs through the formation of hydrogen bonds between the polysaccharide chains, leading to a gel "ordered" state. This process is enhanced by hydrated anions, such as Cl^-, but especially SO_4^{2-}, due to their ability to reduce interactions between water molecules and the hydrophilic sites of the biopolymer, thereby promoting chain–chain associations. It is interesting to note that both the experimental gelling temperature, T_{gel} (solid dots), and the normalized T_{2m} (empty dots), which provides an overview of the degree of dehydration of the network at the end of gelation stage, scale linearly with the hydration entropy of the anion, ΔS_{hydr}, as indicated in the plot. Extrapolation of both T_{gel} (dashed line, y-axis on the left) and T_{2m} (dotted line, y-axis on the right) at $\Delta S_{hydr} = 0$ correlates well with experimental findings of agarose hydrogels in pure deionized water. The values of ΔS_{hydr} indicated in the plot are from the literature [37].
(The cartoon is created in BioRender. Sacco, P. (2026) https://BioRender.com/dzcgyiy.)

molecules around itself [46,47]. This is reflected quantitatively in the hydration entropy, ΔS_{hydr}, of each hydrated anion. The end result is the dehydration of the biopolymer, making it less soluble. In the case of the agarose sample used in this study, it exhibits small amounts (DS = 7.4%) of hydrophobic domains characterized by the presence of *O*-methyl groups at the C_6 position of galactose as determined by ^{1}H- and ^{13}C-HSQC [4]. Therefore, the contribution of hydrophilic hydroxyl groups dominates. In view of these considerations and the fact that the dehydration process is proportional to ΔS_{hydr}, which in our case is - 200 and - 75 J/(mol K) for SO_4^{2-} and Cl^-, respectively [37], we attribute the increase in T_{gel} to the change in the entropy of the hydration water around the hydrophilic sites of agarose, which causes an overall dehydration of the biopolymer with release of water molecules, leading to earlier gelation (Figs. 1 and 2). This is consistent with the low-field NMR data (Fig. 3) as T_{2m} is strictly connected with the water-biopolymer interactions. Fitting the T_{2m} experimental data with a one-phase decay equation allows calculation of the rate constant (see Supplementary Materials), which is approximately 0.23 min^{-1} for all three conditions tested. This indicates that the dehydration process is controlled by ΔS_{hydr}, not by a kinetic contribution, when working at constant agarose concentration and same temperature quenching rate. Overall, the dependence of T_{gel} on ΔS_{hydr} allows extrapolation of the gelling temperature at $\Delta S_{hydr} = 0$, which is very close to the experimental value observed for the T_{gel} of agarose samples in deionized water (40.8 °C experimental *vs.* 40.5 °C theoretical). Similarly, the dependence of normalized T_{2m} on ΔS_{hydr} allows extrapolation of the relaxation time of the proton of water molecules in hydrogels without anions (0.03 experimental *vs.* 0.04 theoretical). Therefore, the combination of T_{gel}, ΔS_{hydr}, and T_{2m} allows to propose a gelling mechanism for agarose in the presence of kosmotropic anions (Fig. 9).

In contrast to alginate hydrogels, where two water-rich microenvironments with different abundancy can be detected at the end of the gelation kinetics [48], it is interesting to note that the dehydration of agarose leads to the formation of a single network when C_p is set to 1% w/V, regardless of the anion used in the process. The whole network becomes heterogeneous when C_p is lowered to 0.5% w/V, when the simultaneous presence of two microenvironments with different hydration in the ratio 80:20% is detected (Supplementary Materials, Fig. S7). This situation is similar to the case of agarose with C_p = 2%, where a ratio of 60:40% between two microenvironments was observed applying Raman optical activity [5]. However, the addition of anions has important effects on the topological evolution of the network (Fig. 4), with Cl^- causing a gradual, but more scattered, exchange between two microenvironments characterized by different amounts of water, while SO_4^{2-} promotes the sudden formation of a hydrated network immediately after an equilibrium phase consisting of two concomitant microenvironments in a 20:80 proportion. This heterogeneous phase can tentatively be correlated with the discontinuity region of the storage modulus shown in Fig. 1a, which is characterized by significant variation in the corresponding phase angle (Supplementary Materials, Fig. S4). These results are also consistent with the cryo-SEM images shown in Fig. 8, which reveal a slightly more heterogeneous architecture of the network for SO_4^{2-}-supplemented hydrogels due to the uncontrolled dehydration of the biopolymer. Taken together, these

results indicate that the macromolecular arrangements of agarose chains during the gelation stage are highly correlated with the concentration of the biopolymer and the nature of the kosmotropic anion used in the experimental setting.

The gelation stage of agarose can also be modulated by changing the concentration of the biopolymer or by applying mechanical stimulation (Figs. 5 and 7). In terms of the amount of agarose, it is not surprising that the increase of T_{gel} is observed with an increase in C_p, and this can be merely interpreted in terms of the overall entanglement throughout the gelling phase. Our results are in line with previous contributions in the field [13,16]. At low concentration of agarose, such as 0.5% w/V, the plateau elastic modulus of the final hydrogel is around 300 Pa, comparable to the discontinuity phase observed for the storage modulus in the gelation curves of more concentrated agarose solutions. Of note, we verified experimentally that the storage modulus of 0.5% w/V hydrogels increases over time up to ~1 kPa if left to rest on the stage of the rheometer. This suggests that the network matures over time if not subjected to external stress. This is consistent with the heterogeneity of the network topology at the end of the gelation stage (Supplementary Materials, Fig. S7). Overall, the effect of C_p on the hydration of the final network is remarkable (Fig. 6), clearly indicating a direct interplay between water and agarose bundles in the formation of a hydrogen bonding system [3]. On the other hand, strain stimulation of agarose leads, to some extent, to modulation of the gelation stage. While T_{gel} is not significantly affected by the amplitude imposed during the temperature sweep, a negative correlation is observed between the plateau elastic modulus and, more importantly, the extent of the discontinuity region of the storage modulus as a function of applied deformation (Fig. 7). In this case, the increase in applied deformation during the oscillatory temperature sweep is expected to align the agarose chains and force their association, likewise what happens for the formation of temporary bonds under shear that induce non-linear elasticity in similar polysaccharide systems [49]. However, our results are not consistent with a previous work in which the increase in amplitude during the oscillatory temperature sweep led to an extension of the discontinuity [14]. This different behaviour could be attributed to a different chemical composition of the agarose used in that study.

While we found a crucial contribution of kosmotropic anions in modulating the gelation stage of agarose, we did not observe substantial differences in the mechanical response of the hydrogels when analyzed at the end of the pseudo-equilibrium stage, especially in terms of elasticity (Fig. 8). This is justified by the very similar hydration of the networks as detected by LF-NMR, with T_{2m} around 130 ms for all conditions tested, and by the similar nano-scale architecture of the network (Supplementary Materials, Fig. S8). It is interesting to observe that, while at the end of the gelation stage there is a clear correlation between the dehydration of the network and the kosmotropic degree of the anion, the differences level off at prolonged timescales, *i.e.* at the end of the pseudo-equilibrium stage. This suggests that a macromolecular rearrangement of the network occurs. In addition, agarose hydrogels are mild sensitive to the ionic strength >1 M generated by the ions. Our results are only partially in agreement with previous studies using gelatin-based hydrogels as model, where the treatment with the highly hydrated SO_4^{2-} anion causes much more significant strengthening of the network, higher fracture elongation, tensile strength and toughness [50,51]. The discrepancy can be partly attributed to the different experimental conditions. Namely, while previous studies used a soaking approach (first assembling the hydrogel and then soaking in the kosmotropic salt), we mixed the anions with agarose solution after autoclaving and then allowed them to gel. However, even when we prepared agarose hydrogels in deionized water and then immersed them in the kosmotropic salts as control experiment, using the same protocol as in other papers, we did not observe significant improvements in the mechanical response of our hydrogels (Supplementary Materials, Fig. S11). For gelatin-based hydrogels, the addition of the highly kosmotropic anion SO_4^{2-} leads to strong hydrophobic interactions and bundling between the gelatin chains, especially when used in large quantities, thus improving the mechanics of the hydrogels. In the case of the agarose used in this study, the contribution of the hydrophobic domains is low, as explained above, which is why a lower sensitivity of agarose hydrogels to mechanical stimulation in relation to the ionic strength is to be expected.

5. Conclusions

In this study, we primarily investigated the role of anions with different degrees of hydration in modulating the gelation stage of a low hydrophobic agarose. The anions play a major role in influencing the gelation temperature of the biopolymer, T_{gel}, and final elasticity of the network, as demonstrated by rheology and SAXS measurements, and this correlates well with the entropy of hydration of the anion, ΔS_{hydr}. The result is an enhanced ability of the SO_4^{2-} anion to weaken the water-biopolymer interactions and dehydrate the hydrophilic groups of agarose compared to Cl^-. This also has implications for the evolution of the network topology, as evidenced by LF-NMR measurements. Our results indicate that gelation transitions from a progressive to a sudden change of two water-rich microenvironments when the kosmotropic nature of the anion is enhanced, suggesting that the gelation of agarose is governed by a more or less controlled self-organization process. However, we have shown that agarose hydrogels exhibit similar mechanics regardless of the type of anion and are not highly sensitive to ionic strength >1 M when analyzed at the end of the pseudo-equilibrium stage. This is justified by a similar amount of water-biopolymer interactions, as evidenced by LF-NMR, the architecture observed by cryo-SEM in the networks at longer time scales and the low amount of hydrophobic domains of the agarose used in this study. The future use of different agarose samples with variable hydrophobicity will provide additional insight into both the gelling mechanism and the sensitivity of the final hydrogels to mechanical stimulation. In this study, we have also secondarily investigated the effects of agarose concentration and mechanical stimulation on the gelation stage. Our results are consistent with previous investigations in the field, indicating a positive correlation between biopolymer concentration and both the gelling temperature and the final elasticity of the hydrogel network. Notably, we demonstrate here that the different water-agarose interplay in the network underlies these findings. Results regarding mechanical stimulation during the gelation stage are much more difficult to interpret and are characterized by higher experimental error. However, rheological data indicate that the imposed strain during measurement decreases the plateau elastic modulus and reduces the discontinuity region of the storage modulus. Further intensive work is required to fully elucidate the molecular basis of this phenomenon.

CRediT authorship contribution statement

Lorenzo Mio: Writing – review & editing, Investigation, Data curation. **Francesco Piazza:** Writing – review & editing, Software, Investigation, Data curation. **Michela Abrami:** Writing – review & editing, Investigation, Data curation. **Martina Conti:** Writing – review & editing, Methodology, Investigation, Data curation. **Francesco Lopez:** Writing – review & editing, Data curation. **Emiliano Fratini:** Writing – review & editing, Supervision, Methodology, Funding acquisition, Data curation. **Mario Grassi:** Writing – review & editing, Methodology, Data curation. **Francesco Brun:** Methodology, Data curation. **Ivan Donati:** Writing – review & editing, Supervision, Project administration, Methodology, Data curation, Conceptualization. **Pasquale Sacco:** Writing – review & editing, Writing – original draft, Supervision, Project administration, Methodology, Funding acquisition, Data curation, Conceptualization.

Declaration of Generative AI and AI-assisted technologies in the writing process

During the preparation of this manuscript, the author Pasquale Sacco used InstaText, an AI-assisted editing tool for language improvement, specifically to improve spelling, grammar, word choice, readability, and clarity. After using this tool, the authors reviewed and revised the text as needed and take full responsibility for the content of the publication.

Declaration of competing interest

The authors declare that they have no known competing financial interests or personal relationships that could have appeared to influence the work reported in this paper.

Acknowledgments

This study was supported by the grant D40-microgrants23_SACCO and by the Fondo Sociale Europeo Plus della Regione Autonoma Friuli Venezia Giulia. The authors gratefully acknowledge the support of the ISIS@MACH ITALIA Research Infrastructure, the hub of ISIS Neutron and Muon Source (UK), [MUR official registry U. 0008642.28-05-2020 – 16th April 2020]. The authors thank the CSGI for partial financial support. This work benefited from the use of the SasView application, originally developed under NSF award DMR-0520547. SasView contains code developed with funding from the European Union's Horizon 2020 research and innovation programme under the SINE2020 project, grant agreement No 654000.

Appendix A. Supplementary data

The online version contains the Supplementary Materials file, which includes: additional figures and data elaboration; SAXS data fitting; LF-NMR data fitting. Raw data generated during this study are available upon reasonable request. Correspondence and requests for materials should be addressed to L. Mio and P. Sacco. Supplementary data to this article can be found online at https://doi.org/10.1016/j.ijbiomac.2026.150233.

Data availability

Data will be made available on request.

References

[1] P. Zarrintaj, S. Manouchehri, Z. Ahmadi, M.R. Saeb, A.M. Urbanska, D.L. Kaplan, M. Mozafari, Agarose-based biomaterials for tissue engineering, Carbohydr. Polym. 187 (2018) 66–84.
[2] C. Araki, Structure of the agarose constituent of agar-agar, Bull. Chem. Soc. Jpn. 29 (4) (1956) 543–544.
[3] S. Arnott, A. Fulmer, W.E. Scott, I.C.M. Dea, R. Moorhouse, D.A. Rees, The agarose double helix and its function in agarose gel structure, J. Mol. Biol. 90 (2) (1974) 269–284.
[4] F. Piazza, P. Sacco, E. Marsich, G. Baj, F. Asaro, G. Grassi, M. Grassi, I. Donati, Cell activities on viscoelastic substrates show an elastic energy threshold and correlate with the linear elastic energy loss in the strain-softening region, Adv. Funct. Mater. 33 (52) (2023) 2307224.
[5] A. Rüther, A. Forget, A. Roy, C. Carballo, F. Mießmer, R.K. Dukor, L.A. Nafie, C. Johannessen, V.P. Shastri, S. Lüdeke, Unravelling a direct role for polysaccharide β-strands in the higher order structure of physical hydrogels, Angew. Chem. Int. Ed. 56 (16) (2017) 4603–4607.
[6] M. Lahaye, C. Rochas, Chemical structure and physico-chemical properties of agar, Hydrobiologia 221 (1) (1991) 137–148.
[7] G.T. Feke, W. Prins, Spinodal phase separation in a macromolecular sol → gel transition, Macromolecules 7 (4) (1974) 527–530.
[8] M. Manno, A. Emanuele, V. Martorana, D. Bulone, P.L. San Biagio, M.B. Palma-Vittorelli, M.U. Palma, Multiple interactions between molecular and supramolecular ordering, Phys. Rev. E 59 (2) (1999) 2222.
[9] M. Matsuo, T. Tanaka, L. Ma, Gelation mechanism of agarose and κ-carrageenan solutions estimated in terms of concentration fluctuation, Polymer 43 (19) (2002) 5299–5309.
[10] J.Y. Xiong, J. Narayanan, X.Y. Liu, T.K. Chong, S.B. Chen, T.S. Chung, Topology evolution and gelation mechanism of agarose gel, J. Phys. Chem. B 109 (12) (2005) 5638–5643.
[11] B. Dai, S. Matsukawa, NMR studies of the gelation mechanism and molecular dynamics in agar solutions, Food Hydrocoll. 26 (1) (2012) 181–186.
[12] M. Martínez-Sanz, A. Ström, P. Lopez-Sanchez, S.H. Knutsen, S. Ballance, H. K. Zobel, A. Sokolova, E.P. Gilbert, A. López-Rubio, Advanced structural characterisation of agar-based hydrogels: rheological and small angle scattering studies, Carbohydr. Polym. 236 (2020) 115655.
[13] Z.H. Mohammed, M.W.N. Hember, R.K. Richardson, E.R. Morris, Kinetic and equilibrium processes in the formation and melting of agarose gels, Carbohydr. Polym. 36 (1) (1998) 15–26.
[14] D. Nordqvist, T.A. Vilgis, Rheological study of the gelation process of agarose-based solutions, Food Biophys. 6 (4) (2011) 450–460.
[15] C.T. Buckley, S.D. Thorpe, F.J. O'Brien, A.J. Robinson, D.J. Kelly, The effect of concentration, thermal history and cell seeding density on the initial mechanical properties of agarose hydrogels, J. Mech. Behav. Biomed. Mater. 2 (5) (2009) 512–521.
[16] V. Normand, D.L. Lootens, E. Amici, K.P. Plucknett, P. Aymard, New insight into agarose gel mechanical properties, Biomacromolecules 1 (4) (2000) 730–738.
[17] F. Piazza, P. Parisse, J. Passerino, E. Marsich, L. Bersanini, D. Porrelli, G. Baj, I. Donati, P. Sacco, Controlled quenching of agarose defines hydrogels with tunable structural, bulk mechanical, surface nanomechanical and cell response in 2d cultures, Adv. Healthc. Mater. 12 (26) (2023) 2300973.
[18] M. Watase, K. Arakawa, Rheological properties of hydrogels of agar-agar. III. Stress relaxation of agarose gels, Bull. Chem. Soc. Jpn. 41 (8) (1968) 1830–1834.
[19] M. Watase, K. Nishinari, Rheological properties of agarose gels with different molecular weights, Rheol. Acta 22 (6) (1983) 580–587.
[20] X. Gong, C. Lin, J. Cheng, J. Su, H. Zhao, T. Liu, X. Wen, P. Zhao, Generation of multicellular tumor spheroids with microwell-based agarose scaffolds for drug testing, PLoS One 10 (6) (2015) e0130348.
[21] M.A. Krishnan, K. Yadav, V. Chelvam, Agarose micro-well platform for rapid generation of homogenous 3D tumor spheroids, Curr. Protoc. 1 (7) (2021) e199.
[22] M. Li, T. Fu, S. Yang, L. Pan, J. Tang, M. Chen, P. Liang, Z. Gao, L. Guo, Agarose-based spheroid culture enhanced stemness and promoted odontogenic differentiation potential of human dental follicle cells in vitro, In Vitro Cell. Dev. Biol. Anim. 57 (6) (2021) 620–630.
[23] M.C. Dodla, R.V. Bellamkonda, Differences between the effect of anisotropic and isotropic laminin and nerve growth factor presenting scaffolds on nerve regeneration across long peripheral nerve gaps, Biomaterials 29 (1) (2008) 33–46.
[24] Y. Luo, M.S. Shoichet, A photolabile hydrogel for guided three-dimensional cell growth and migration, Nat. Mater. 3 (4) (2004) 249–253.
[25] Y. Luo, M.S. Shoichet, Light-activated immobilization of biomolecules to agarose hydrogels for controlled cellular response, Biomacromolecules 5 (6) (2004) 2315–2323.
[26] F. Piazza, B. Ravaglia, A. Caporale, A. Svetić, P. Parisse, F. Asaro, G. Grassi, L. Secco, R. Sgarra, E. Marsich, I. Donati, P. Sacco, Elucidating the unexpected cell adhesive properties of agarose substrates. The effect of mechanics, fetal bovine serum and specific peptide sequences, Acta Biomater. 189 (2024) 286–297.
[27] N. Rahman, K.A. Purpura, R.G. Wylie, P.W. Zandstra, M.S. Shoichet, The use of vascular endothelial growth factor functionalized agarose to guide pluripotent stem cell aggregates toward blood progenitor cells, Biomaterials 31 (32) (2010) 8262–8270.
[28] P. Sacco, F. Piazza, C. Pizzolitto, G. Baj, F. Brun, E. Marsich, I. Donati, Regulation of substrate dissipation via tunable linear elasticity controls cell activity, Adv. Funct. Mater. 32 (29) (2022) 2200309.
[29] Y. Yamada, K. Hozumi, A. Aso, A. Hotta, K. Toma, F. Katagiri, Y. Kikkawa, M. Nomizu, Laminin active peptide/agarose matrices as multifunctional biomaterials for tissue engineering, Biomaterials 33 (16) (2012) 4118–4125.
[30] Y. Yamada, C. Yoshida, K. Hamada, Y. Kikkawa, M. Nomizu, Development of three-dimensional cell culture scaffolds using laminin peptide-conjugated agarose microgels, Biomacromolecules 21 (9) (2020) 3765–3771.
[31] M. Djabourov, A.H. Clark, D.W. Rowlands, S.B. Ross-Murphy, Small-angle X-ray scattering characterization of agarose sols and gels, Macromolecules 22 (1) (1989) 180–188.
[32] M. Jaspers, A.E. Rowan, J. Kouwer, P. H., Tuning hydrogel mechanics using the Hofmeister effect, Adv. Funct. Mater. 25 (41) (2015) 6503–6510.
[33] S. Meiboom, D. Gill, Modified spin-echo method for measuring nuclear relaxation times, Rev. Sci. Instrum. 29 (8) (1958) 688–691.
[34] M.M. Chui, R.J. Phillips, M.J. McCarthy, Measurement of the porous microstructure of hydrogels by nuclear magnetic resonance, J. Colloid Interface Sci. 174 (2) (1995) 336–344.
[35] N.R. Draper, H. Smith, Applied Regression Analysis, John Wiley & Sons, Ltd, 1966.
[36] T.N. Blanton, T.C. Huang, H. Toraya, C.R. Hubbard, S.B. Robie, D. Louër, H. E. Göbel, G. Will, R. Gilles, T. Raftery, JCPDS—International Centre for Diffraction Data round robin study of silver behenate. A possible low-angle X-ray diffraction calibration standard, Powder Diffract. 10 (2) (1995) 91–95.
[37] B.A. Deyerle, Y. Zhang, Effects of Hofmeister anions on the aggregation behavior of PEO-PPO-PEO triblock copolymers, Langmuir 27 (15) (2011) 9203–9210.
[38] W. Wei, Hofmeister effects shine in nanoscience, Adv. Sci. 10 (22) (2023) 2302057.
[39] H. Jung, L.C. Geonzon, W.B. Yoon, S. Matsukawa, Change of network structure in agarose solution during gelation studied by multiple particle tracking and NMR measurements, Food Hydrocoll. 141 (2023) 108740.
[40] G. Ferraro, E. Fratini, P. Sacco, F. Asaro, F. Cuomo, I. Donati, F. Lopez, Structural characterization and physical ageing of mucilage from chia for food processing applications, Food Hydrocoll. 129 (2022) 107614.

[41] R. Mastrangelo, C. Resta, E. Carretti, E. Fratini, P. Baglioni, Sponge-like cryogels from liquid-liquid phase separation: structure, porosity, and diffusional gel properties, ACS Appl. Mater. Interfaces 15 (39) (2023) 46428–46439.
[42] T. Singh, R. Meena, A. Kumar, Effect of sodium sulfate on the gelling behavior of agarose and water structure inside the gel networks, J. Phys. Chem. B 113 (8) (2009) 2519–2525.
[43] P. Sacco, F. Piazza, E. Marsich, M. Abrami, M. Grassi, I. Donati, Ionic strength impacts the physical properties of agarose hydrogels, Gels 10 (2) (2024) 94.
[44] P. Bertsch, P. Sacco, The role of non-linear viscoelastic hydrogel mechanics in cell culture and transduction, Mater. Today Bio 34 (2025) 102188.
[45] K.B. Rembert, J. Paterová, J. Heyda, C. Hilty, P. Jungwirth, P.S. Cremer, Molecular mechanisms of ion-specific effects on proteins, J. Am. Chem. Soc. 134 (24) (2012) 10039–10046.
[46] H. Muta, S. Kawauchi, M. Satoh, Ion effects on hydrogen-bonding hydration of polymer an approach by 'induced force model', J. Mol. Struct. (THEOCHEM) 620 (1) (2003) 65–76.
[47] H. Muta, M. Miwa, M. Satoh, Ion-specific swelling of hydrophilic polymer gels, Polymer 42 (14) (2001) 6313–6316.
[48] G. Turco, I. Donati, M. Grassi, G. Marchioli, R. Lapasin, S. Paoletti, Mechanical spectroscopy and relaxometry on alginate hydrogels: a comparative analysis for structural characterization and network mesh size determination, Biomacromolecules 12 (4) (2011) 1272–1282.
[49] F. Furlani, A. Marfoglia, E. Marsich, I. Donati, P. Sacco, Strain hardening in highly acetylated chitosan gels, Biomacromolecules 22 (7) (2021) 2902–2909.
[50] Q. He, Y. Huang, S. Wang, Hofmeister effect-assisted one step fabrication of ductile and strong gelatin hydrogels, Adv. Funct. Mater. 28 (5) (2018) 1705069.
[51] J. Li, H.L. Chee, Y.T. Chong, B.Q.Y. Chan, K. Xue, P.C. Lim, X.J. Loh, F. Wang, Hofmeister effect mediated strong PHEMA-gelatin hydrogel actuator, ACS Appl. Mater. Interfaces 14 (20) (2022) 23826–23838.

Supplementary Materials

Effect of anions, concentration and mechanical stimulation on the gelation of agarose

Lorenzo Mio [1], Francesco Piazza [2], Michela Abrami [3], Martina Conti [4], Francesco Lopez [5], Emiliano Fratini [6], Mario Grassi [3], Francesco Brun [3], Ivan Donati [2], and Pasquale Sacco [2,]*

[1] Department of Medicine, Surgery and Health Sciences, University of Trieste, 34129 Trieste, Italy

[2] Department of Life Sciences, University of Trieste, Via Licio Giorgieri 5, I-34127, Trieste, Italy

[3] Department of Engineering and Architecture, University of Trieste, Via A. Valerio 6/1, I-34127 Trieste, Italy

[4] CNR-Istituto Officina dei Materiali (IOM), SS 14 km 163.5, Area Science Park Basovizza, Trieste, 34149, Italy

[5] Department of Agricultural, Environmental and Food Sciences (DiAAA) & CSGI, Università degli Studi del Molise, Via De Sanctis, I-86100 Campobasso, Italy.

[6] Department of Chemistry "Ugo Schiff" & CSGI, University of Florence, Via della Lastruccia 3, 50019 Sesto Fiorentino (FI), Florence, Italy.

* Corresponding Author

Tel: +39 040 558 8731

e-mail: psacco@units.it

Additional Figures.

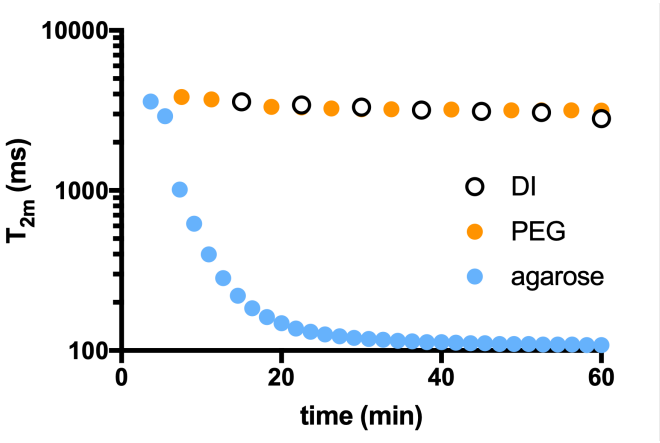

Figure S1. Validation of low-field NMR for the evaluation of agarose gelation. Upon quenching at $T = 25$ °C from $T = 60$ °C, the average relaxation time (T_{2m}) of deionized water (DI) and the PEG solution, used as control, decreases to a limited extent due to the reduction in temperature. In contrast, the decrease in T_{2m} of the agarose (1% w/V, deionized water as solvent) solution is much more pronounced as it is due to both cooling and hydrogel formation, a process that involves a large increase in solid surface area (agarose chain) per unit volume. The large difference in the decrease of T_{2m} in the case of the agarose compared to that of deionized water and PEG solution emphasizes the importance of LF-NMR to follow the gelation of the biopolymer.

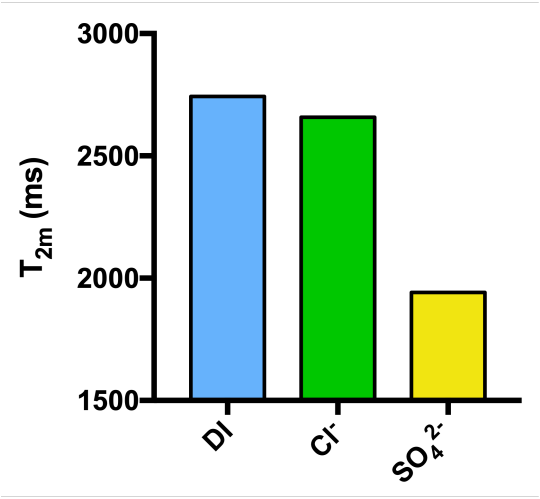

Figure S2. Dependence of the medium relaxation time, T_{2m}, as a function of deionized water (DI) or anion (Cl^- or SO_4^{2-}) solutions, as solvent. The low-field NMR experiments were performed at $T = 25$ °C. In the case of anion solutions, the ionic strength, I, is kept constant at 1 M, considering also the contribution of the respective counterions (Na^+ for chloride and NH_4^+ for sulphate).

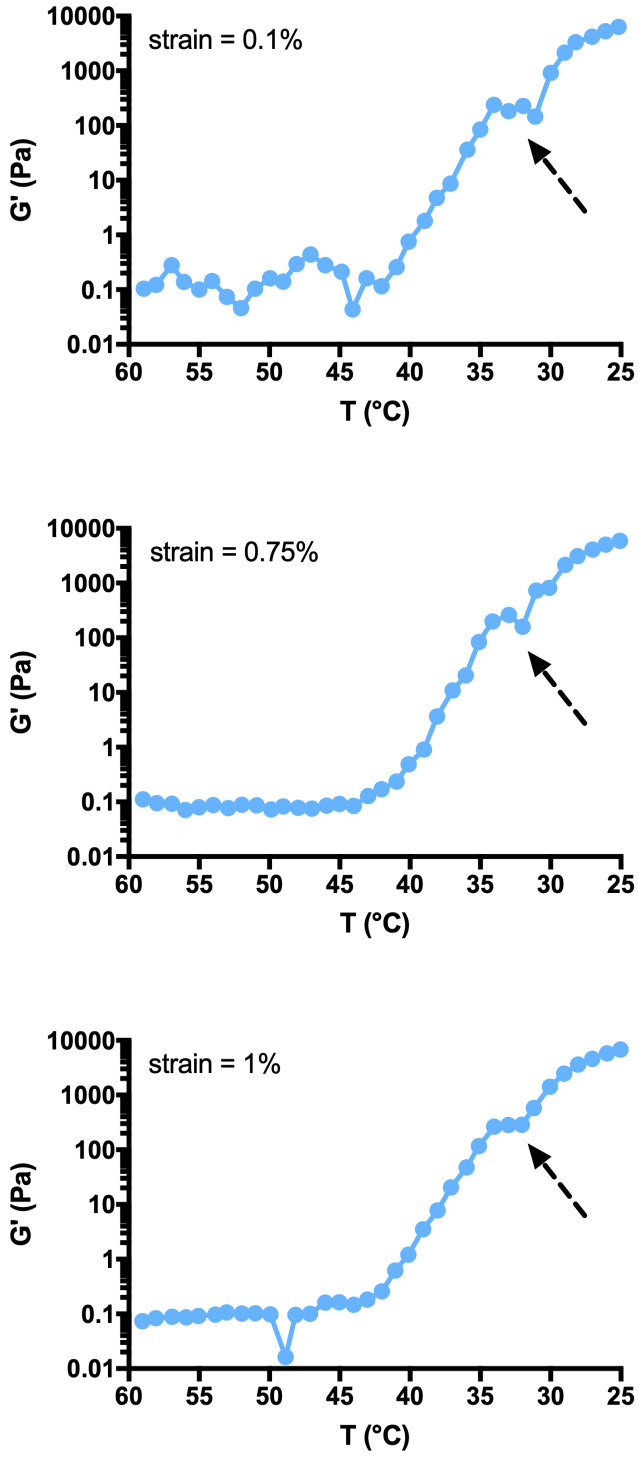

Figure S3. Sample-case temperature sweep curves of agarose using different strains. The solid blue lines represent the experimental values of the elastic modulus, G', as a function of temperature. The black arrows indicate the discontinuity region. The temperature sweep experiments were performed with variable strain indicated in plots, a frequency of 1 Hz and a cooling rate of 1 °C/min. Composition of samples: [agarose] = 1% w/V; deionized water as solvent.

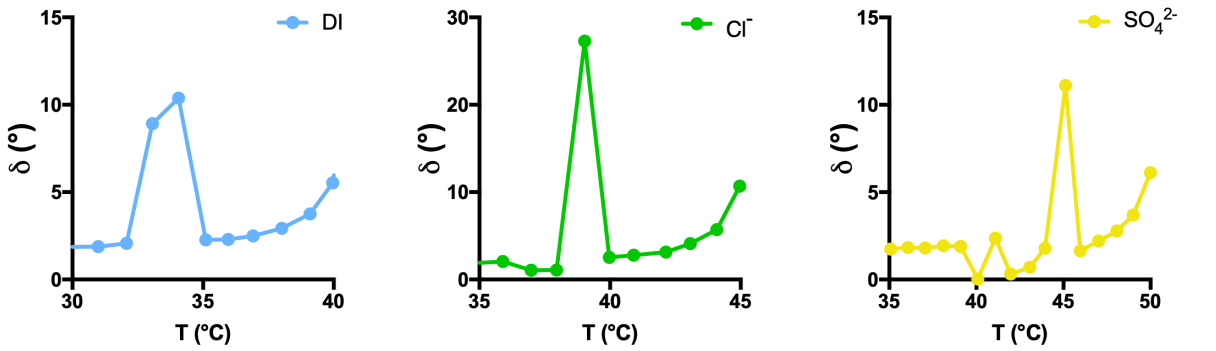

Figure S4. Phase angle, δ (°), response during the temperature-sweep experiments of agarose in the absence or presence of anions Cl^- or SO_4^{2-}. The temperature range shown in the plots includes the discontinuity region observed in Figure 1a of the main manuscript. The oscillatory temperature sweep experiments were performed with a constant strain of 0.5%, a frequency of 1 Hz and a cooling rate of 1 °C/min. Composition of samples: [agarose] = 1% w/V; deionized water (DI) or anion (Cl^- or SO_4^{2-}) solutions, as dispersing phase. In the case of anion solutions, the ionic strength, *I*, is kept constant at 1 M, considering also the contribution of the respective counterions (Na^+ for chloride and NH_4^+ for sulphate).

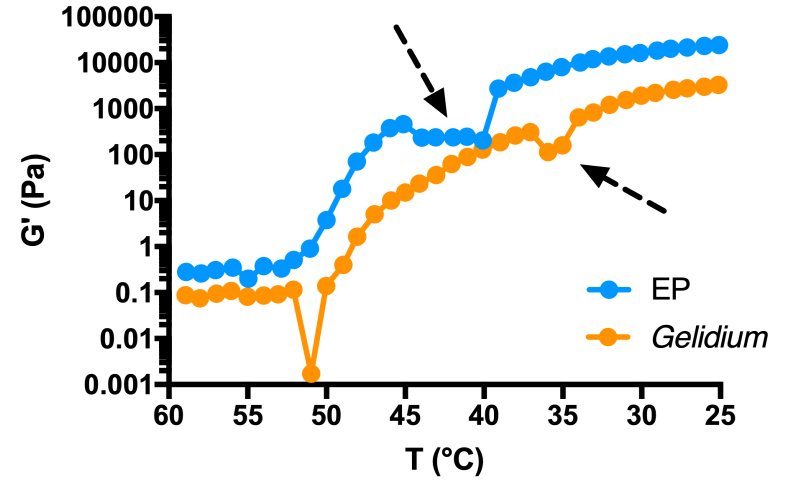

Figure S5. Elastic response of agaroses with different chemical composition. Agarose for electrophoresis (EP) and agarose from *Gelidium* are compared. See paragraph 2.1 in the main manuscript for a complete overview of the physicochemical characteristics of the biopolymers. The oscillatory temperature sweep experiments were performed with a constant strain of 0.5%, a frequency of 1 Hz and a cooling rate of 1 °C/min. Composition of samples: [agarose, EP or *Gelidium*] = 1% w/V; $(NH_4)_2SO_4$ as dispersing phase, with final ionic strength, *I*, of 1 M. The black arrows indicate the discontinuity region.

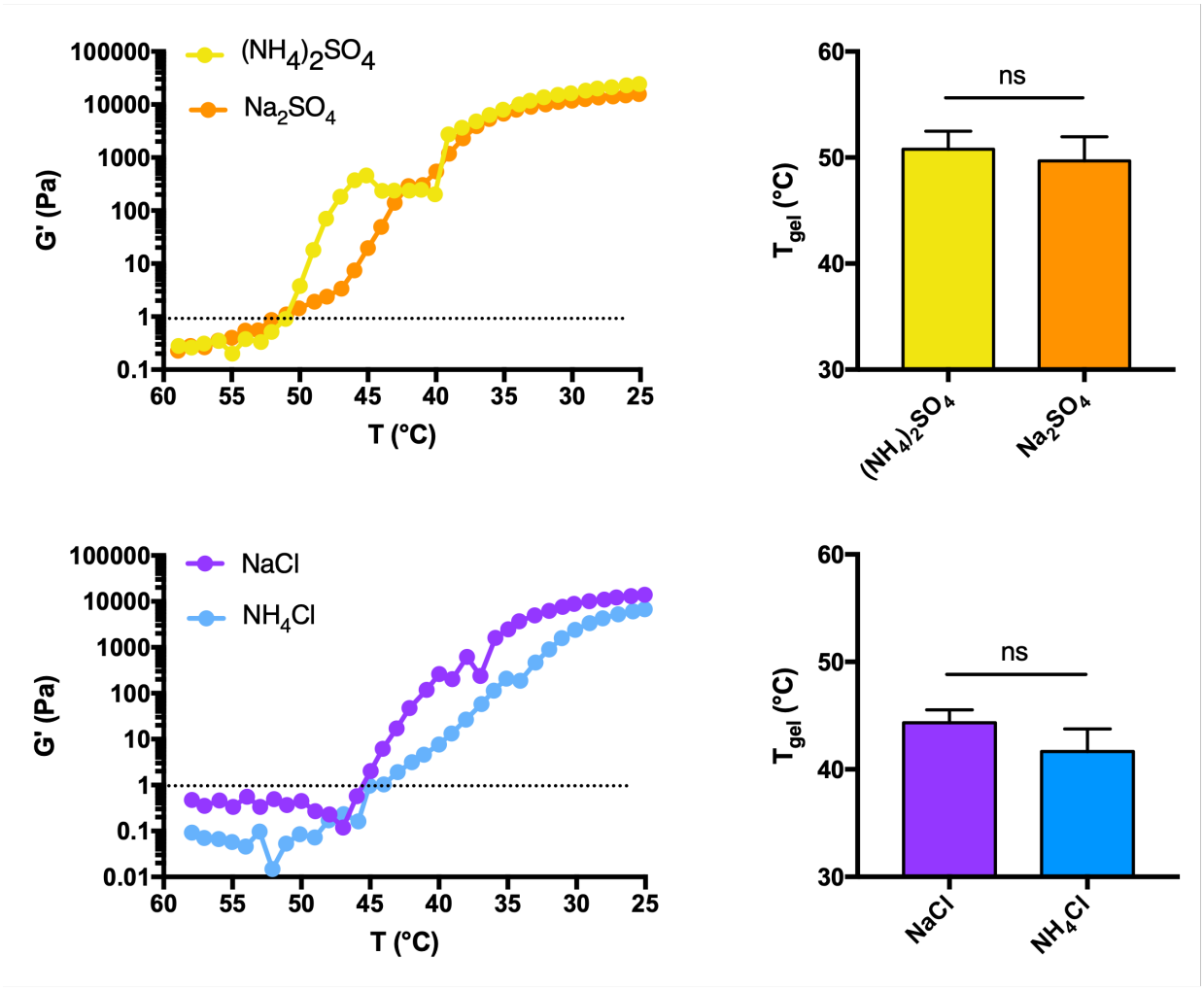

Figure S6. (Left) Sample-case temperature sweep curves of agarose in the presence of different salts. The solid dots and lines represent the experimental values of the storage modulus, G'. The dotted line is set at 1 Pa and marks the baseline for the calculation of T_{gel}. (Right) Bar graphs indicating the temperature at which the gelation of agarose in the presence of different salts starts, T_{gel}; data are given as mean ± SD, n = 3 - 4 samples analyzed for each experimental condition. Statistics: ns, not significant; Mann-Whitney test for the case of $(NH_4)_2SO_4$ *vs.* Na_2SO_4 and unpaired t test for the case of NaCl *vs.* NH_4Cl. The oscillatory temperature sweep experiments were performed with a constant strain of 0.5%, a frequency of 1 Hz and a cooling rate of 1 °C/min. Composition of samples: [agarose] = 1% w/V; salt solutions as dispersing phase. The ionic strength, I, is 1 M for all conditions tested.

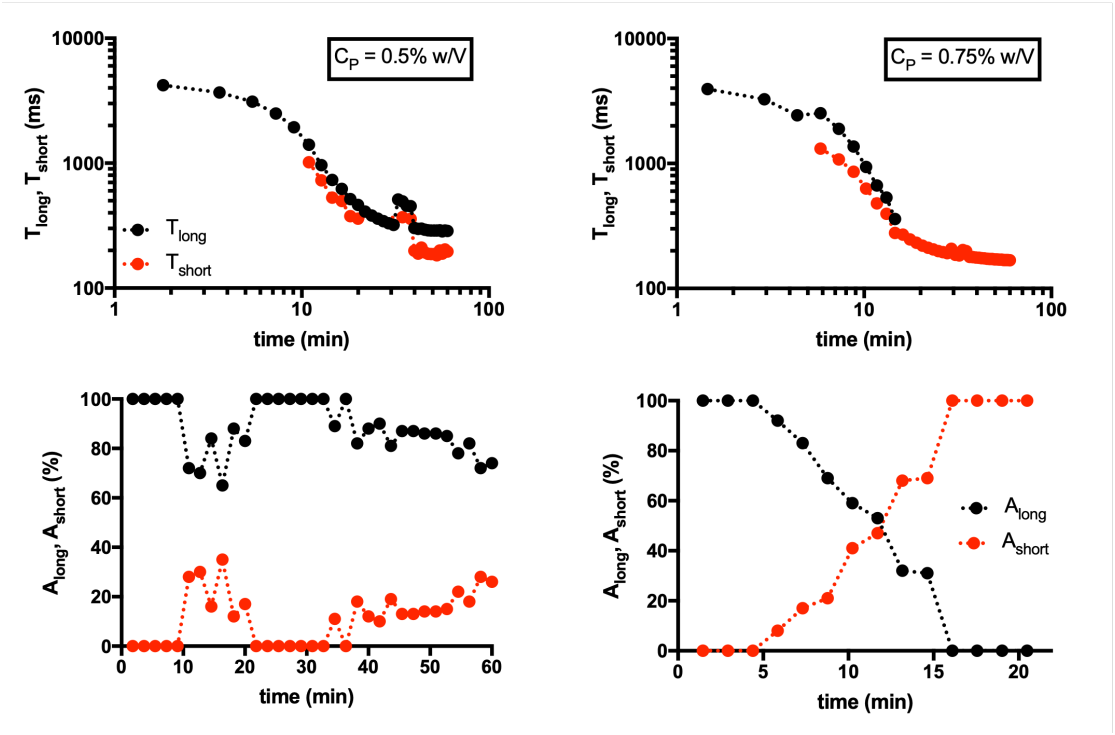

Figure S7. Upper row: dependence of the long (T_{long}) and short (T_{short}) relaxation time during the hydrogel formation; dotted lines are drawn to guide the eye. Lower row: variation of the spin density of the signal in relation to the long (A_{long}) and short (A_{short}) relaxation times; the lines are drawn to guide the eye. The low-field NMR experiments were performed immediately quenching the samples at $T = 25$ °C. Composition of samples: [agarose] = 0.5 or 0.75% w/V; deionized water (DI) as solvent.

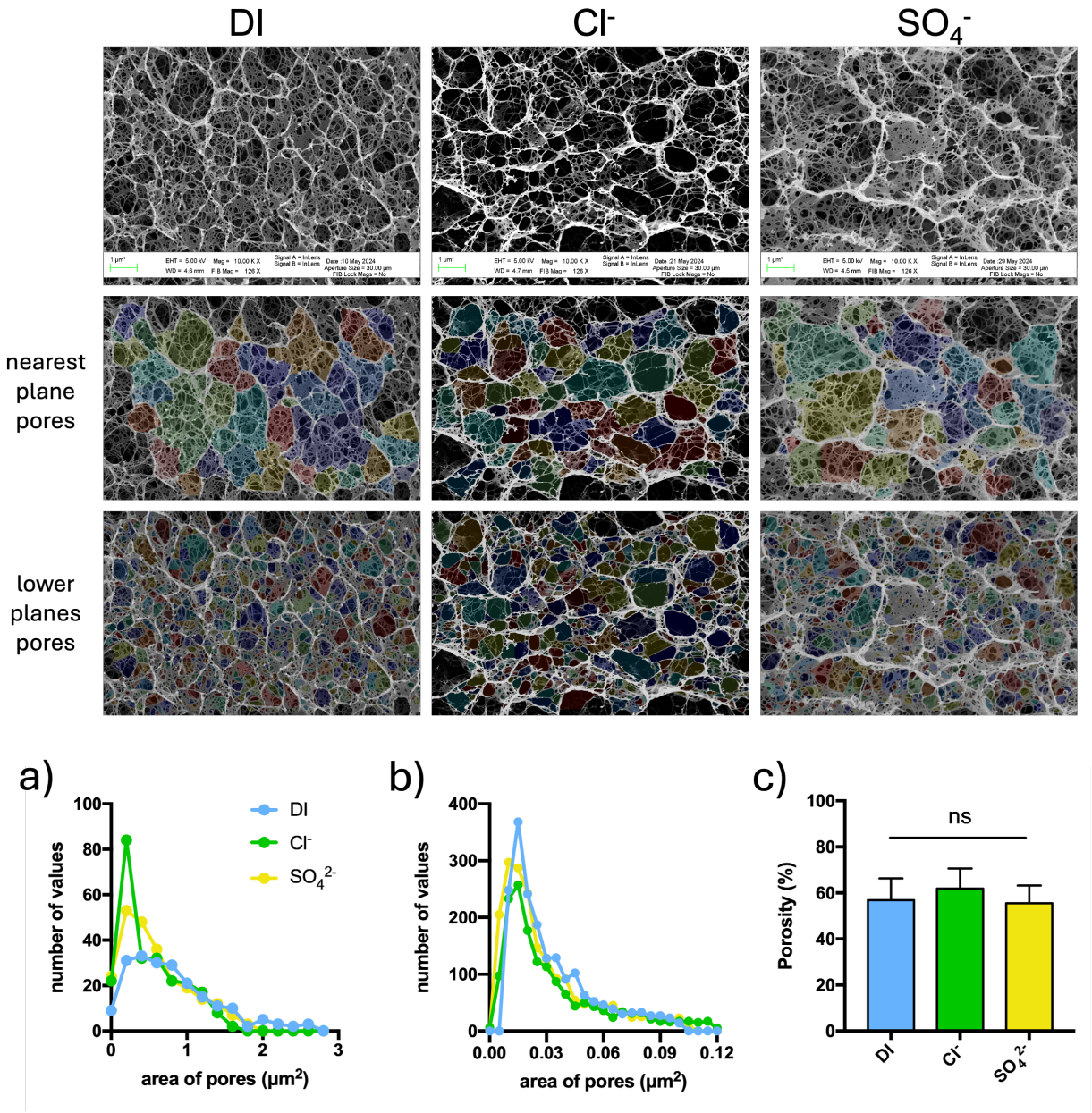

Figure S8. Upper row: representative cryo-SEM images for each case; middle and lower rows: results of automatic region recognition, with each detected area superimposed on the corresponding image using pseudocolors. The area of each identified region was quantified and reported in the frequency distribution graphs: (a) distribution of pore area in the nearest plane; (b) distribution of pore area in the lower planes. The average global porosity value for each group was also calculated following global thresholding and is summarized in the bar graph (c); data are given as mean ± SD, $n = 4$ images analyzed for each experimental condition. At least 35 pores have been analyzed for each image. Statistics: ns, not significant; One-way ANOVA followed by Tukey's Multiple Comparisons test.

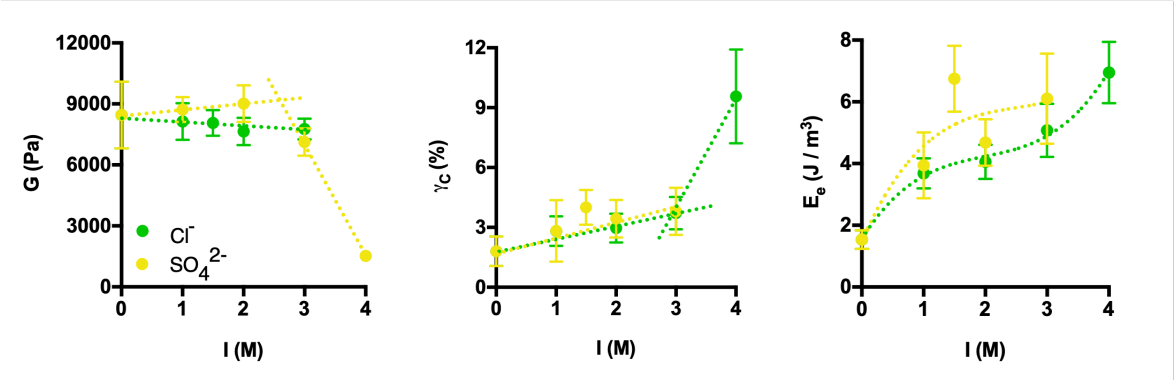

Figure S9. Dependence of the shear modulus, G, the critical strain which marks the end of stress-strain linear region, γ_c, and the elastic energy, E_e, calculated at γ_c as a function of ionic strength, I; data are given as mean ± SD for G and γ_c, and mean ± SEM for E_e, n = 6 - 14 hydrogels analyzed for each experimental condition. The lines are drawn to guide the eye. Composition of hydrogels: [agarose] = 1% w/V; anion (Cl^- or SO_4^{2-}) solutions. The ionic strength was varied considering also the contribution of the respective counterions (Na^+ for chloride and NH_4^+ for sulphate).

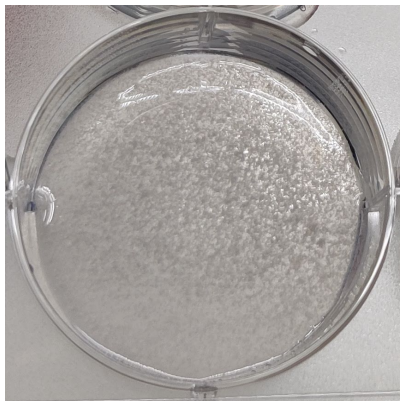

Figure S10. Salting-out of agarose 1% w/V in the presence of $(NH_4)_2SO_4$, with final ionic strength, I, of 4 M.

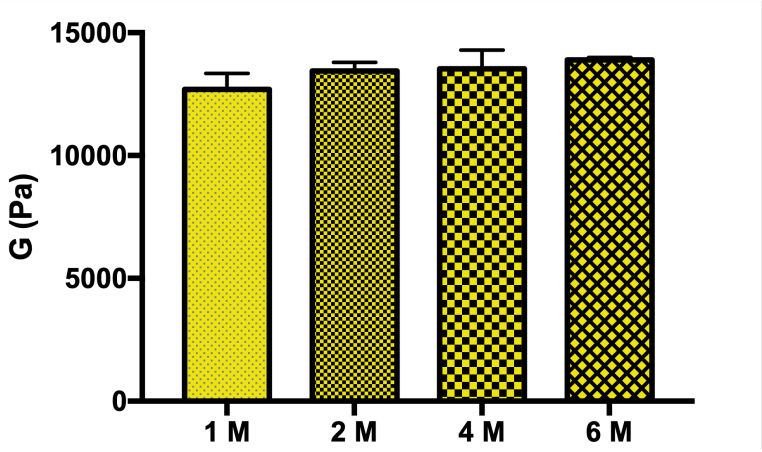

Figure S11. Soaking agarose hydrogels (1% w/V, deionized water as solvent) in $(NH_4)_2SO_4$ producing different ionic strengths, *I* (M). The shear modulus is indicated on the y-axis of the graph and was used to compare the mechanical response of the different conditions tested. Data are given as mean ± SD, *n* = 3 - 8 samples analyzed for each experimental condition.

SAXS data fitting.

The nanoscale structure of the final agarose hydrogel can be described by a model that includes two q-dependent terms.[1,2] The first term (*i.e.* Lorenz term) describes the rapid fluctuations of the polymer chains in a liquid-like state while the second term (*i.e.* Guinier term) accounts for the solid-like regions associated to the static accumulations of cross-linking regions and polymer clusters:

$$I(q) = A\left\{\frac{I_L(0)}{(1+[(D+1)/3]q^2\xi^2)^{D/2}} + I_G(0)\exp\left(q^2R_g^2/3\right)\right\} + bkg \qquad \text{(eq. S1)}$$

where A is a scaling factor taking into account the instrumental set-up; $I_L(0)$ and $I_G(0)$ are the Lorenz and Guinier contributions at q = 0 nm^{-1}; D is the fractal dimension connected to the conformation of the polymer chains (*i.e.* bad, good or θ-solvent state) which persists over an average correlation length of ξ (*i.e.* blob/mesh size); R_g is the Guinier radius (*i.e.* the average dimension of the solid-like region) and *bkg* is a q-independent contribution describing the incoherent/parasitic scattering.

	DI	Cl^-	SO_4^{2-}
$I_G(0)$	9.2 ± 0.2	7.0 ± 0.1	15.9 ± 0.6
$I_L(0)$	5.6 ± 0.1	6.9 ± 0.1	9.9 ± 0.2
R_g (nm)	32.5 ± 0.3	29.8 ± 0.3	38.0 ± 0.4
D	3.2 ± 0.1	3.0 ± 0.1	3.1 ± 0.1
ξ (nm)	7.2 ± 0.1	8.4 ± 0.1	10.1 ± 0.1

Table S1. Structural parameter extracted by the fit of the scattering curves reported in Figure 8e-g of the main manuscript according to the eq. S1.

Low-field NMR data fitting.

Experimental data for the normalized medium relaxation time of the proton of water molecules, T_{2m}, as reported in Figure 3 of the main manuscript, can be fitted using eq. S2, where $T_{2m\to 0}$ is the medium relaxation time at time zero, c is the plateau of T_{2m} at infinite time, and k is the rate constant expressed in min^{-1}.

$$T_{2m} = (T_{2m\to 0} - c)e^{-kt} + c \qquad \text{(eq. S2)}$$

An example of fitting experimental data is shown in the figure below, where the black dots represent the experimental points and the solid red line is the best fit obtained using equation S2.

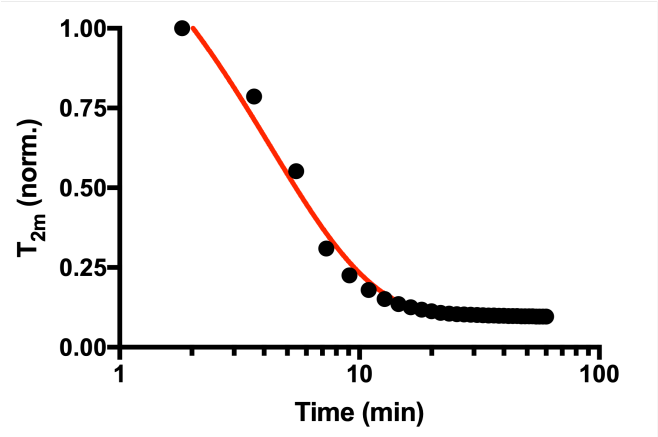

	DI	Cl^-	SO_4^{2-}
$T_{2m,\ t\ =\ 0}$	1.64 ± 0.11	1.55 ± 0.03	1.56 ± 0.05
$k\ (min^{-1})$	0.22 ± 0.02	0.23 ± 0.01	0.24 ± 0.01
c	0.02 ± 0.01	0.06 ± 0.01	0.10 ± 0.01
R^2	0.96	0.99	0.99

Table S2. Structural parameter extracted by the fit of normalized T_{2m} curves reported in Figure 3 of the main manuscript according to the eq. S2.

References

(1) Mallam, S.; Horkay, F.; Hecht, A. M.; Rennie, A. R.; Geissler, E. Microscopic and Macroscopic Thermodynamic Observations in Swollen Poly(Dimethylsiloxane) Networks. *Macromolecules* **1991**, *24* (2), 543–548.

(2) Shibayama, M.; Tanaka, T.; Han, C. C. Small-angle Neutron Scattering Study on Weakly Charged Temperature Sensitive Polymer Gels. *J Chem Phys* **1992**, *97* (9), 6842–6854.